Manuscript Click here to view linked References

Performance of packed-bed thermal energy storage using recycled aggregate: From a lab-scale prototype to a 1 MWh module

Liuhui Tu, Vithushanthini Arulkumar, Guillermo A. Narsilio, Tuan Nguyen[1]

Department of Infrastructure Engineering, The University of Melbourne, VIC 3010, Australia

Abstract

Recycled aggregate (RA) is produced during construction and demolition activities, but its reuse is limited by residual mortar content and the energy-intensive thermal treatment required. Using RA as a filler in packed-bed thermal energy storage (PBTES) offers a dual function: acting as a sensible heat-storage medium and supporting RA thermal treatment, which enhances material recovery and circularity. This study explores a concept of concrete circularity-renewable energy symbiosis through a case study of RA-PBTES with dual functions. Laboratory experiments assessed the thermal response, pressure drop, cyclic repeatability, and structural behaviour of RA-PBTES under repeated heating and cooling. Results showed RA maintained stable thermocline development, good heat storage, and acceptable hydraulic resistance, though some thermal ratcheting occurred at 250°C, emphasising the need to consider particle movement and bed structure for long-term design. Repeated thermal cycling made RA particles more brittle, suggesting benefits for crushing and residual mortar removal. To explore scalability, a one-dimensional heat-transfer model based on the Schumann formulation was developed and validated, accurately predicting temperature and thermocline development obtained from the experiments. Applying this model to a 1 MWh storage module assessed large-scale thermal performance, fan energy, and system behaviour, revealing trade-offs among heat transfer, resistance, energy use, and material utilisation. The use of waste-derived RA further offers potential sustainability benefits through material reuse and subsequent thermal upgrading.

Keywords: Packed bed thermal energy storage; Recycled aggregate; Thermocline; Pressure drop; Thermo-mechanical response; Energy storage system

1 Introduction

This section presents the background and motivation of the study, focusing on thermal energy storage for renewable energy. It reviews its role in solar power and low-carbon systems, then narrows to packed-bed storage and recycled aggregate as a medium. Research gaps, objectives, and scope are outlined.

[1] Corresponding author. E-mail address: tuan.nguyen@unimelb.edu.au (Tuan Nguyen).

1.1 Background

Governments worldwide are actively pursuing the swift decarbonisation of electricity systems. In Australia, this transition is particularly significant, as the Australian Government aims to achieve 82% renewable energy by 2030 [1]. To fully transition to renewable electricity, the share of solar energy could be considerably increased by deploying additional Concentrating Solar Power (CSP) facilities. In a typical CSP system, thermal energy storage (TES) is a crucial component [2, 3], as it stores excess energy during times of high renewable production and release it during periods of high demand or low generation, thereby greatly improving grid stability, reliability, and flexibility [4].

The available TES methodologies can be classified into sensible, latent, and thermochemical approaches based on the physical principle used to store heat [5, 6]. Sensible TES systems can be classified as active or passive [7]. In an active system, a heat transfer fluid (HTF) serves as both a heat transport medium and a TES medium, whereas in a passive system, it serves only as a heat transport medium [8]. A packed-bed (PB) TES system uses the thermal capacity of a bed of packed particulate material or packing elements (PEs) to store thermal energy, which is exchanged via heat convection with an HTF that flows through the PBTES system [9, 10]. PBTES systems can be configured as either fixed beds or moving beds. In a fixed-bed system, the solid storage particles remain stationary while the heat transfer fluid passes through the bed to charge and discharge thermal energy. In contrast, in a moving-bed system, the solid particles themselves move through the system, enabling direct heat exchange between the particles and the heat transfer fluid [11, 12]. PBTES is attractive for large-scale renewable-energy storage because of its relatively simple configuration, direct heat transfer, broad operating-temperature range, and potential use of low-cost solid fillers [13]. Nevertheless, the sustainability of a PBTES system depends not only on its thermal efficiency, but also on the origin, embodied carbon impacts, durability, and end-of-life (EoL) pathway of the storage material [14, 15]. Large-scale deployment using quarried rock or manufactured ceramic media may create additional demand for virgin resources and energy-intensive processing. Incorporating secondary materials recovered from industrial or construction waste streams could reduce reliance on virgin fillers while retaining material value within productive use [16, 17]. Accordingly, selecting PB media provides an opportunity to embed circular-economy principles directly into renewable-energy storage infrastructure.

1.2 Conventional and waste-derived packed-bed materials

Filler selection is a key consideration in PBTES design because it directly affects heat-storage capacity, heat-transfer behaviour, pressure drop, mechanical stability, system cost, and operating-temperature range. Conventional packed-bed materials generally include natural rocks and manufactured ceramic elements. Natural rocks are widely used because of their availability, low cost, and relatively high thermal stability, whereas ceramic packing elements can provide more controlled geometry, porosity, and flow distribution [18]. Metallic fillers offer higher thermal conductivity and faster heat transfer [9], but their high cost, density, embodied energy, and potential corrosion may limit their suitability for large-scale storage. [19]

Using recycled waste materials as filler media in PBTES systems offers an eco-friendly, cost-effective way to enhance thermal performance while reducing environmental impact [20, 21]. Demolition waste heated at 120~180 °C using synthetic oil as HTF in a pilot-scale solar heat system showed an energetic efficiency of over 95% and a total system efficiency of 66.6% [22]. Mining by-products such as Porcellanitic achieved charge and discharge efficiencies of 87% and 88%, respectively, in large-scale systems designed for industrial waste-heat recovery [23]. Asbestos-containing waste has shown a thermal efficiency of 82% when compared to traditional alumina packing, with significantly faster charging (12%) and discharging (16%) with synthetic oil up to 300 °C [24]. Electric arc furnace slag [12] and steel slag [13] have also shown efficiencies of 70–74%. Copper slag and metallurgical steel slag [25] were shown to reduce molten salt volume by 31.4% in hybrid two-tank systems [26]. Larger-scale applications using recycled ceramic [27] achieved a thermal exergy efficiency of 88% in CSP fields [28]. These studies collectively highlight the promising role of waste materials in enhancing the environmental profile and functional performance of PBTES.

The literature above therefore shows that waste-derived materials can provide competitive thermal-storage performance and serve as viable alternatives to conventional packed-bed fillers. Existing research has extensively investigated key thermo-hydraulic aspects of PBTES, including heat-transfer behaviour, pressure drop across the bed, particle characteristics, and overall system performance. However, comparatively few studies have examined the long-term evolution of waste-derived filler materials under repeated thermal cycling, particularly mechanical degradation, particle breakage, fines generation, and post-use condition.

1.3 Advances in recycled aggregate for thermal applications

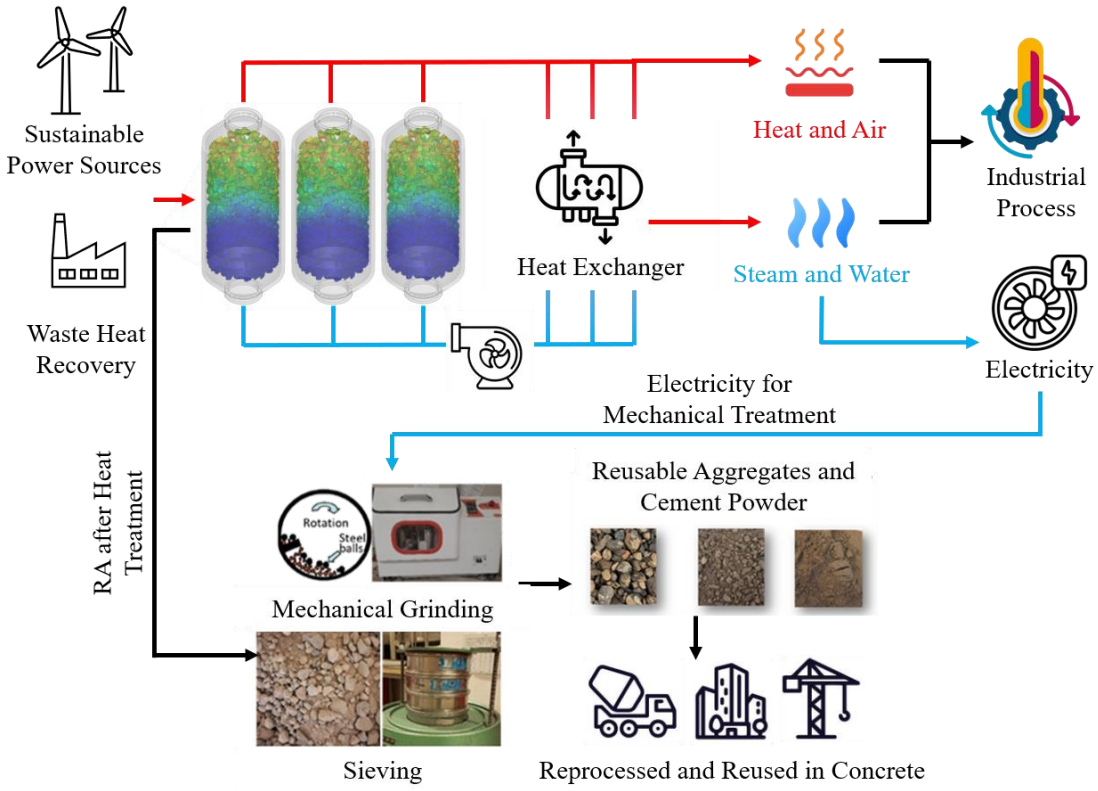
Construction and demolition waste (C&D) accounts for more than 30% of total solid waste worldwide [29], representing a significant opportunity for the filler media of PBTES [30] while representing an application for diverting a higher portion of C&D waste from landfills than others proposed in the literature (e.g., in concrete [31], in pavements [32, 33], etc.). Recycled aggregate (RA) accounts for about 60 to 70 % of all recycled materials from C&D waste [34]. In addition to its widespread availability and low acquisition cost, RA possesses thermal-storage characteristics that support its potential use as a sensible-heat filler in moderate-temperature PBTES systems.

Previous studies indicate that RA can retain acceptable bulk integrity within the temperature range typically considered for low- to medium-temperature thermal storage. It exhibits sufficient thermal and structural stability for use in thermal energy storage systems operating at moderate temperatures under 300 °C, with significant changes in the dehydration of cement present in the attached mortar starting to occur around 350 °C [35]. RA retains its bulk integrity, and thermal cycling within this range does not significantly compromise physical properties [36]. Beyond its direct use as a sensible-heat filler, researchers have also incorporated recycled concrete and demolition-waste-derived materials into other TES configurations. Ramón-Álvarez et al. [37] recently demonstrated an eco-efficient cementitious single-tank TES concept incorporating recycled construction and demolition waste as the internal filler, with the

cementitious tank wall providing structural support while also contributing to sensible heat storage. Under repeated air-based thermal cycling between 30 and 180 °C, the CDW-filled systems showed discharge performance comparable to systems packed with volcanic rock. In parallel, researchers have exploited the porous mortar fraction of recycled concrete aggregate for PCM impregnation. Abden et al. [38] developed PCM-impregnated RCA composite concrete, achieving a latent heat storage capacity of approximately 9.2 J/g and improved thermal regulation compared with conventional RCA concrete. Collectively, these findings support the broader thermal-storage potential of RA and provide a practical basis for its use as a low-cost and sustainable sensible-heat filler in moderate-temperature PBTES.

While numerous efforts have aimed to develop alternative filler materials for PBTES, systematic research on using RA in this context remains limited. The thermal behaviour of RA in actual PBTES setups remains a significant gap in current knowledge. Numerous challenges and inquiries remain to be addressed. The high porosity and water absorption of RA can significantly influence its thermal performance [39], thereby slowing heat transfer and leading to a thicker thermocline. The presence of attached mortar and weak interfacial transition zones (ITZs) can reduce mechanical strength and increase susceptibility to particle degradation under repeated thermal cycling [40]. Conversely, controlled thermal exposure may also create opportunities for subsequent material upgrading [41, 42]. The degradation of RA particles during thermal cycling can facilitate the weakening and detachment of adhered mortar, and PBTES operation may serve as a pretreatment stage that improves the efficiency of downstream thermal–mechanical recycling (TMR) [43], enabling easier material recovery and potentially reducing processing energy demand. These findings suggest a potential connection between thermal-energy storage and RA upgrading [44]. During service in a PBTES system, RA can first function as a sensible-heat storage medium

137 (



138

139 Figure 1). Repeated thermal exposure may then progressively alter or weaken the attached
140 mortar and aggregate–mortar interfaces, potentially reducing the effort required for
141 downstream mechanical processing [45, 46]. In this way, the storage stage could provide a
142 preliminary conditioning effect before crushing, mortar separation, and further material
143 recovery [47].

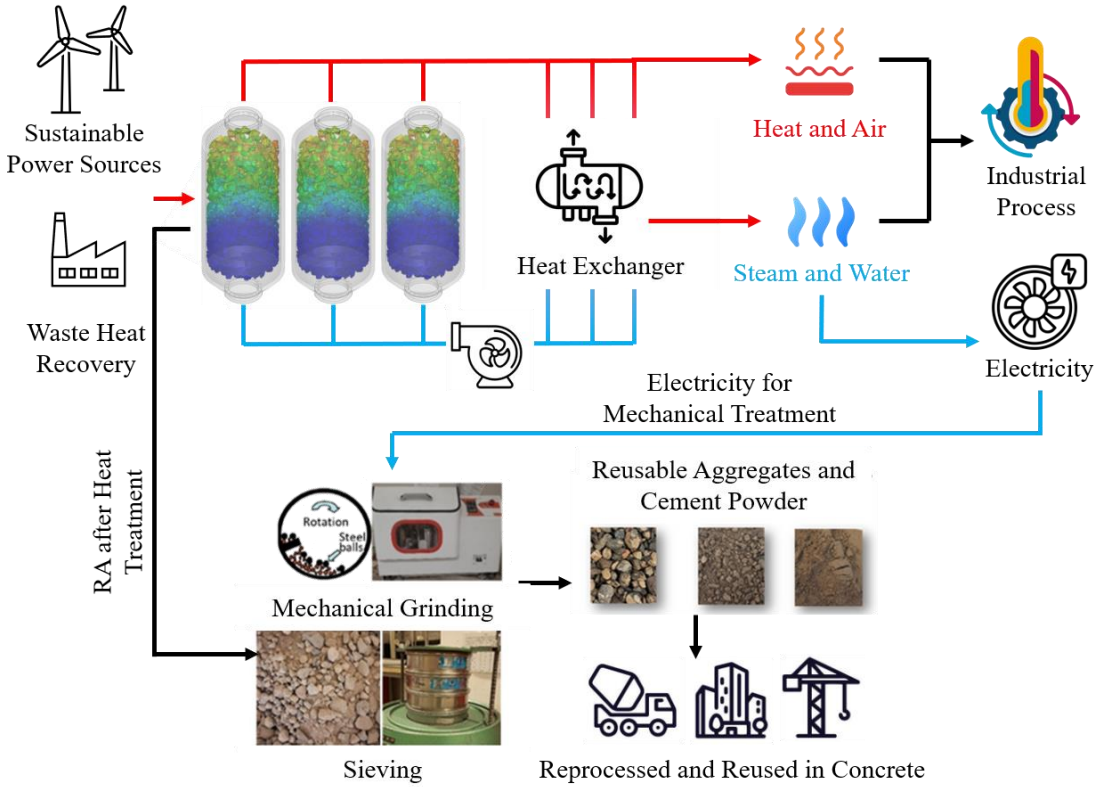


Figure 1 Conceptual framework for the integration of RA-PBTES

However, thermal exposure may also create operational challenges during storage, as repeated heating and cooling can alter particle integrity, thermophysical properties, and packed-bed structure, potentially affecting long-term thermal and hydraulic performance [48]. Repeated expansion and contraction induced by temperature fluctuations may exacerbate existing microcracks and weaken the particle structure, potentially contributing to bed settlement and tank deformation, like the ratcheting effect [49]. The high porosity and water absorption of RA can influence its thermal response [50], while heat transfer and thermal gradients may weaken particle interfaces and increase susceptibility to cracking, fines generation, and changes in particle-size distribution under repeated cycling [51]. Furthermore, the inherent heterogeneity of RA, including variations in density, composition, and internal structure [52], can lead to non-uniform thermal behaviour within the packed bed. These challenges highlight the need for dedicated experimental investigations to advance the understanding and reliable application of RA in PBTES systems. A comprehensive evaluation of RA-PBTES must therefore consider not only thermal-storage performance, but also hydraulic stability, particle durability, structural response, and the condition of the material after service.

1.4 Motivation and contributions of this study

Based on the preceding review, several research gaps remain. First, although researchers have investigated a range of waste-derived materials as PBTES fillers, experimental studies on RA remain limited, particularly under repeated heating and cooling. Second, most existing studies focus primarily on thermal performance, whereas the coupled thermal, hydraulic, and mechanical behaviour of heterogeneous packed beds, including particle rearrangement, bed

settlement, and tank deformation, has received comparatively little attention. Third, the scalability of RA-PBTES systems and the associated trade-offs among heat-transfer performance, pressure loss, fan energy demand, and material utilisation remain insufficiently quantified. Finally, the potential role of thermal storage as an intermediate stage within a broader RA upgrading and material-recovery pathway has not been systematically discussed.

To address these gaps, this study investigates the thermal, hydraulic, mechanical, and system-level performance of an RA-PBTES system through laboratory experiments and analytical modelling. The principal contributions are:

1. Experimental characterisation of RA-PBTES under repeated thermal cycling, including temperature evolution, thermocline development, cyclic repeatability, pressure drop, and tank deformation.
2. Identification of the coupled effects of particle size and material characteristics on thermal discharge behaviour, hydraulic resistance, and packed-bed stability.
3. Experimental observation and discussion of thermo-mechanical ratcheting and particle degradation, highlighting their implications for long-term operation and potential downstream RA processing.
4. Development and validation of a one-dimensional Schumann-based heat-transfer model, followed by scale-up analysis of a 1 MWh RA-PBTES module.
5. System-level evaluation of thermal performance, fan energy demand, and material utilisation, providing engineering insights into the performance and scalability of large-scale RA-PBTES systems.

The study is organised as follows: Section 2 covers the experimental procedure, including the storage materials used, the detailed design of the lab-scale prototype, the testing methodology, the sensor layout, and the data acquisition process, and concludes by defining key performance indicators for evaluation. Section 3 presents the core findings and progressively analyses the temperature distribution, thermocline development, pressure-drop behaviour, and the tank's thermo-mechanical response. Section 4 includes a scale-up analysis linking laboratory observations to potential large-scale applications. Finally, Section 5 summarises the main findings and contributions.

2 Materials, Experimental System and Performance Evaluation

This section describes the materials, experimental system, test procedures, and data-processing methods used to evaluate the packed-bed thermal energy storage system's performance. The section first presents the physical and thermophysical characteristics of the recycled aggregate and benchmark filler material, followed by a description of the laboratory-scale PBTES prototype. The paper then introduces the thermal cycling procedure, operating conditions, and experimental configurations. The sensor arrangement and data-acquisition system are then

described, along with definitions and calculation methods for the thermal, hydraulic, and thermo-mechanical performance indicators used in the analysis.

2.1 Recycled aggregate and benchmark material

In this study, RA was primarily investigated as the filler of the PBTES system, while steel furnace slag (SFS) was also tested as a benchmark filler material. RA denotes a porous cement-based recycled material with irregular morphology, whereas steel slag is a dense, crystalline industrial by-product with higher mechanical strength and thermal conductivity. Figure 2 presents the RA and SFS materials used in this study.



(a) RA-a (19~37.5 mm) (b) RA-b (9.5~19.5 mm) (c) SFS (9.5~19.5 mm)

Figure 2 Recycled Aggregates (RA) (a) 19~37.5 mm, (b) 9.5~19 mm and SFS (c) 9.5~19.5 mm, were used as the filler material for the experimental study

The RA used in this study was from demolished pile caps at a residential development [43]. These caps, part of a structure demolished after about 3 months due to design changes, were made with Grade 50 concrete using ordinary Portland cement, washed river sand, and crushed basalt. The end-of-life concrete was pre-processed on-site with a jackhammer to break it into 20-100 mm pieces. Then, RA was sieved into two size ranges: 19~37.5 mm (RA-a) and 9.5~19.5 mm (RA-b). Steel slag was supplied from Australian Steel Mill Services (ASMS) as single-sized 14 mm aggregate (SFS), with a typical grading ranging from 9.5 to 19 mm [53]. The density of the RA is 2461 kg/m^3 [45] with a water absorption of 3.2%, and the SFS has a particle density of 3 300 kg/m^3 and a water absorption of 1.7%, according to the provided material data sheet [53].

The thermal properties of RA were experimentally measured using a Hot Disk TPS 2 500. The thermal conductivity of RA is 1.49 W/(m·K). The thermal diffusivity is 0.36 mm²/s, and the volumetric specific heat capacity is 4.12 MJ/m³·K. Because this study could not experimentally measure the thermal properties of SFS, it adopted literature values for consistency. According to previous studies [54], the thermal conductivity of SFS is taken as 1.75 W/(m·K). The thermal diffusivity is reported to be approximately 0.82 mm²/s, while the volumetric specific heat capacity is in the range of 2.70 MJ/(m³·K).

2.2 Lab-scale PBTES prototype

In this study, the lab-scale PBTES system contains two major components for straightforward setup and operation: an AISI 201 cylindrical storage tank (Φ 200 mm × 500 mm, 1 mm thickness) with filler material positioned on a mobile support frame with wheels for easy positioning, and an integrated piping system with a three-way joint that manages hot air inflow and outflow from a heating unit. The heating unit is an Industrial Hot Air Blower (RY-P/R-3A) from Shanghai Reyou Machinery Equipment Co., Ltd. (China), with a 0.3 kW fan and a 3 kW/7 kW heating module (

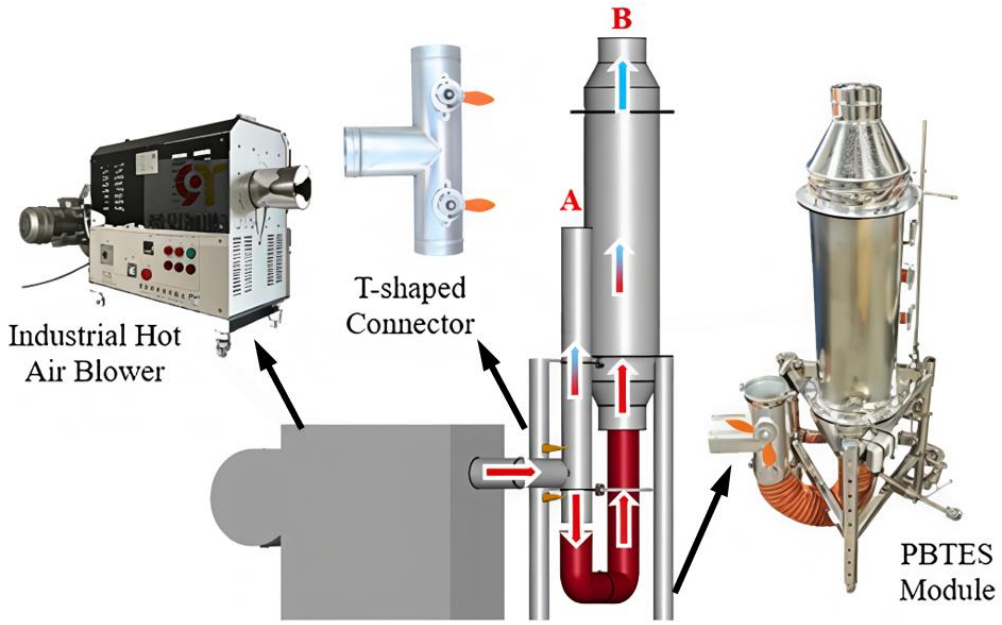


Figure 3).

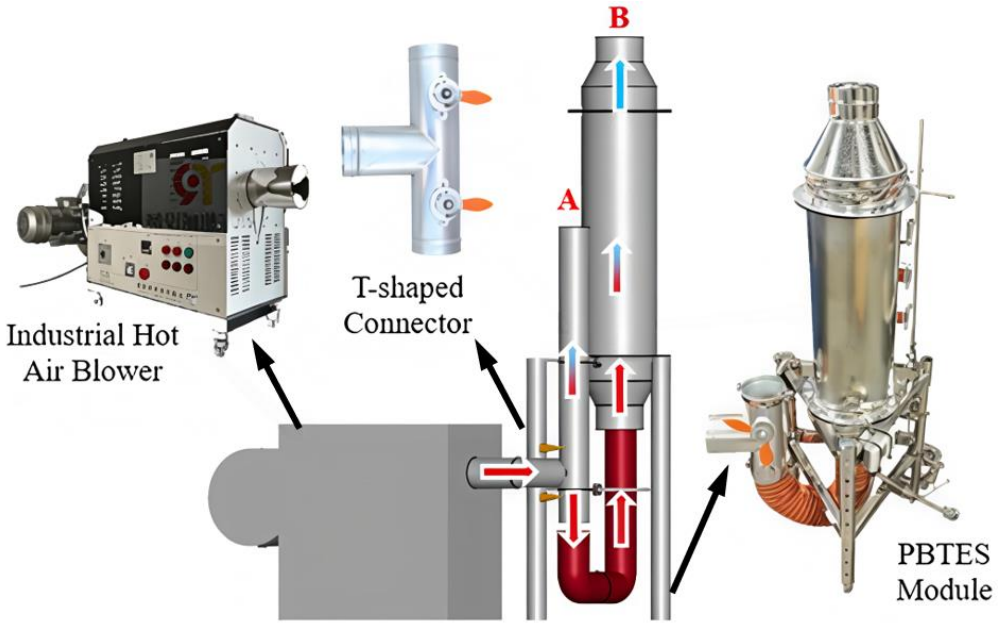


Figure 3 Schematic of the lab-scale prototype, piping system, valve arrangement, and instrumentations

The same flow path was used for both thermal charging and discharging in the present laboratory-scale setup. During charging, hot air entered the tank from the lower inlet and flowed upward through the packed bed; during discharging, ambient air was introduced through the same inlet and followed the same upward flow direction. This configuration was adopted because the heater was directly connected and sealed to the inlet piping, and reversing the flow direction between charging and discharging would have required disassembling the heated connection and reconfiguring the airflow path between cycles. The co-flow arrangement therefore allowed repeated charging–discharging tests to be conducted consistently without disturbing the packed bed or experimental setup. During discharge, the incoming cool air first interacts with the hottest lower region of the bed, causing the lower section to cool earlier while the upper region discharges later. As the air continues upward, its temperature may exceed that of the relatively cooler upper layers, allowing some of the heat extracted from the lower region to redistribute within the bed before reaching the outlet. Consequently, the discharge temperature profile differs from that of a conventional reverse-flow thermocline configuration [55].

2.3 Test Procedure and Cyclic Protocol

The experimental program consisted of four test groups (RA-a1, RA-a2, RA-b, and SFS) designed to evaluate the performance of different filler materials in a PBTES system (Table 1).

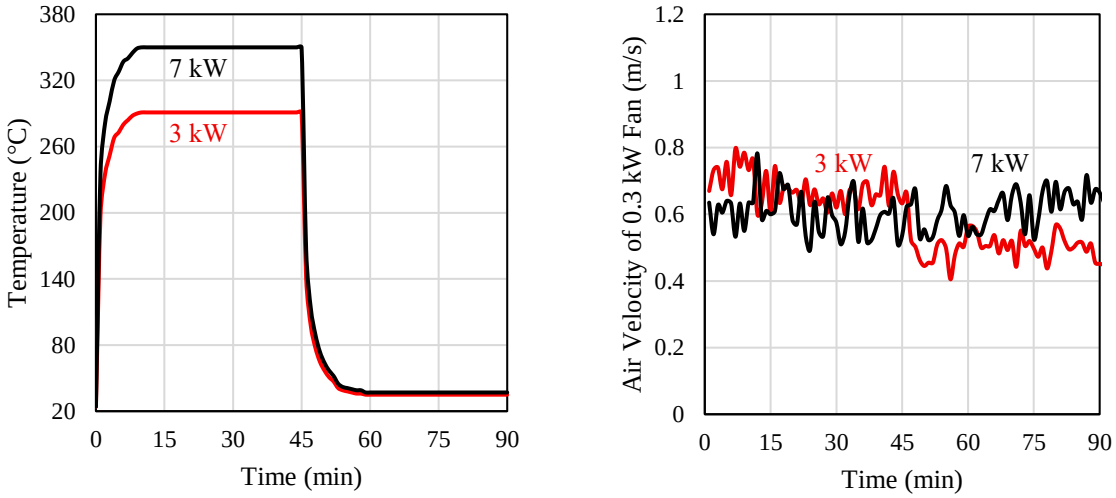
Table 1 The test groups designed for the PBTES with RA and SFS

Test Group	RA-a1	RA-a2	RA-b	SFS
Particle Size (mm)	19~37.5	19~37.5	10~19	10~19
Bed Void Fraction	58%	58%	52%	48%
Target Inlet Air Temperature (°C)	160	250	160	160
Heating Power (kW)	3	7	3	3

All experiments were conducted under comparable operating conditions, with charging and discharging durations set to 45 minutes and fan power fixed at 0.3 kW. An electric heater provided thermal charging by supplying hot air. For the RA-a1, RA-b, and SFS tests, the heating power was 3 kW, targeting an inlet air temperature of 160 °C. The inlet-air temperature increased rapidly during the initial heating period and subsequently approached this operating level rather than remaining constant throughout the charging process. In contrast, the RA-a2 test intentionally employed a higher heating power of 7 kW to achieve a target inlet-air temperature of 250 °C. This case was designed to extend the operating-temperature range while keeping the same RA particle size and bed configuration as RA-a1, enabling assessment of how elevated charging temperature affects storage performance. This experimental design enables a systematic investigation of the effects of filler type, particle size, and operating temperature on the thermal performance and operational behaviour.

Figure 4 presents the operating conditions of the PBTES experiments, including the heating module set temperature at different heating powers. As shown in Figure 4(a), the heating module temperature increases rapidly during the initial heating stage and stabilises at the target

values. At 3 kW, the air temperature stabilises at 291 °C, whereas at 7 kW it stabilises at approximately 350 °C. After the heating stage, the temperature drops rapidly once the heater is turned off, indicating the transition to the cooling phase. Figure 4(b) shows the measured air velocity corresponding to a fan power of 0.3 kW. The air velocity remains relatively stable throughout the experiment, fluctuating around 0.6 m/s.



(a) Temperature of the Heating Module (b) Air Velocity

Figure 4 The set temperature (a) and the power consumption for the blower at relatively constant air velocity (b) of ~0.6 m/s

2.4 Data Acquisition and Sensor Placement

The PBTES system was instrumented with multiple temperature, pressure, and displacement sensors to capture the spatial and temporal thermo-hydraulic behaviour of the storage tank (Figure 5). Eight K-type thermocouples (TC1–TC8, JXWRN-XYQ, Taizhou Suou Electric Heating Appliances Co., Ltd., China, 0.01 K) were installed to monitor the axial and radial temperature evolution within the storage bed. Six thermocouples (TC1–TC6) were positioned along the tank's vertical centreline to measure the axial temperature distribution and thermocline development. The sensors were evenly distributed across the effectively packed region, with reduced spacing near the lower section to capture the initial propagation of the thermal front from the inlet. Two additional thermocouples (TC7 and TC8) were installed on the tank surface at mid-height, radially offset from the centre line, to assess tank surface temperature and potential effects on wall heat loss.

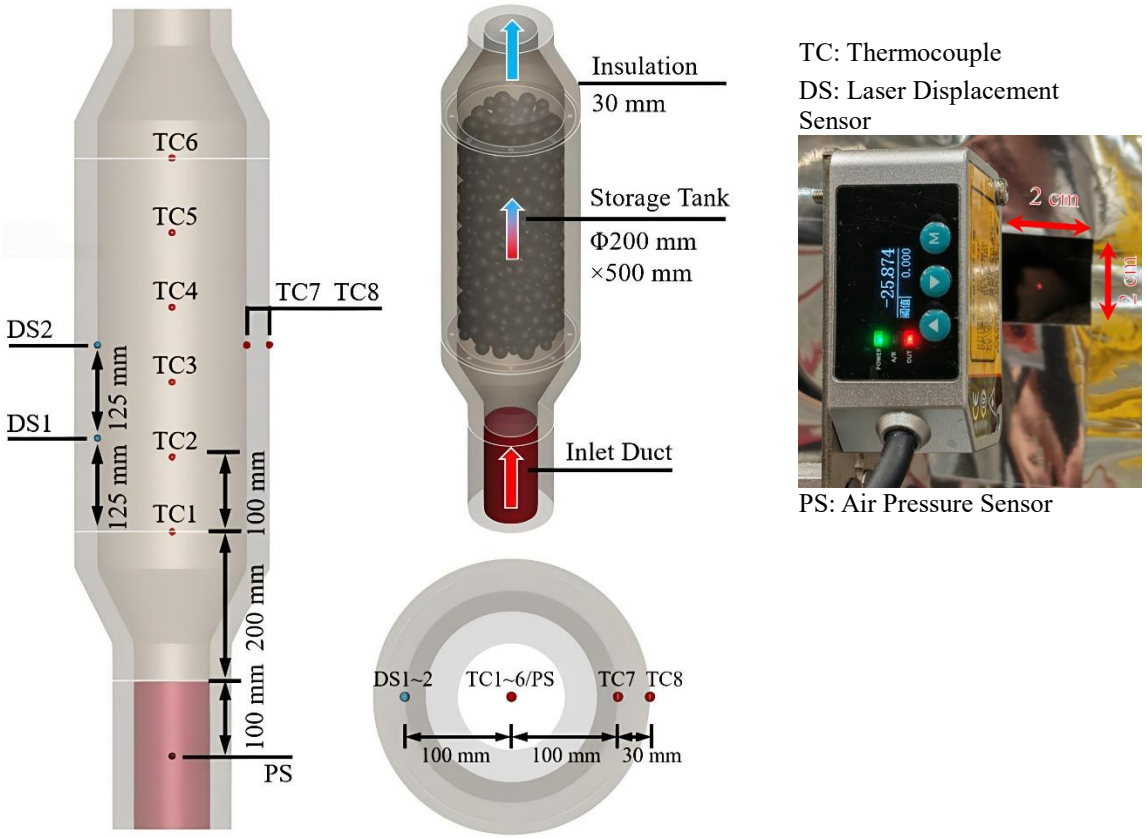


Figure 5 Data Acquisition and sensor placement of the PBTES

An air pressure sensor (PS, SLD-PTG, Nanjing Shunlaida Measurement and Control Equipment Co., Ltd., China, ±0.1 Pa) was installed at the inlet duct to measure the inlet pressure. Three laser displacement sensors (DS1–DS2, ZML-100N-AT, Foshan Zhiman Electronics Co., Ltd., China, resolution 70 μm) were mounted on independent external brackets adjacent to the storage tank's vertical wall at different heights. As shown in Figure 5, to enable direct measurement of tank wall deformation, small openings (2 cm × 2 cm) were created in the insulation layer (30 mm Earthwool [56]), allowing the laser beams to target the steel tank surface directly. The sensors continuously monitored radial displacement during operation, capturing potential structural deformation or thermal expansion at elevated temperatures. These openings locally exposed the tank surface and may have introduced additional heat loss during operation. However, given their small size relative to the overall insulated surface area, the associated effect on the measured system-level thermal performance was expected to be limited.

2.5 Performance Metrics

The key performance indicators (KPIs) described below were used to evaluate the performance of the storage systems for packing materials. Several KPIs, listed and defined in Table 2 were investigated to analyse the thermodynamic performance of the TES and compare different designs in the literature.

Table 2 Key performance indicators for this study

KPI	Definition	Unit	Eq. No
Energy storage capacity [20]	$Q_{max} = (1-\varepsilon)V_{tank}\rho_s \int_{T_{cold}}^{T_{hot}} c_{p,s}(T)dT$	J	(1)
Thermal energy storage density [20]	$Q'''_{max} = \frac{Q_{max}}{V_{tank}}$	kWh/m^3	(2)
Discharging Power [9]	$\dot{Q}_{dis} = \dot{m}_f \left(\int_{T_{in}}^{T_{out}} c_{p,f}(T) d\,T \right)$	W	(3)
Cut-off temperatures [57]	$T_{cut} = T_{cold} + 0.1(T_{hot} - T_{cold})$	°C	(4)
Discharging time [58]	The time interval for the T_{outlet} to drop T_{cut}	min	(5)
Thermocline thickness [58]	Temperature gradient region: $0.1 \leq \frac{T(z)-T_{cold}}{T_{hot}-T_{cold}} \leq 0.9$	mm	(6)
Pressure drop	$\Delta P = P_{inlet} - P_{atm}$	Pa	(7)

*Note: All symbols used other than the KPIs in this table are defined as follows:

ε is the bed porosity (Table 1)
V_{tank} is the volume of the storage tank (m³)
ρ_s is the density of filler material (kg/m³)
$\dot{m}_f$ is the mass flow rate of fluid (kg/s)
$c_{p,s}(T)$ is the temperature-dependent specific heat capacity of solid (J/kg·K)
$c_{p,f}(T)$ is the temperature-dependent specific heat capacity of fluid (J/kg·K)
T_{in} is the inlet fluid temperature (°C)
T_{out} is the outlet fluid temperature (°C)
P_{inlet} is the inlet pressure (Pa)
P_{atm} is the atmospheric pressure (Pa)

To enable consistent comparison between different experiments, T_{hot} is defined as 160 °C (RA-a1, b and SFS) and 250 °C (RA-a2) and T_{cold} is defined as 30 °C.

3 Experimental Results and Discussion

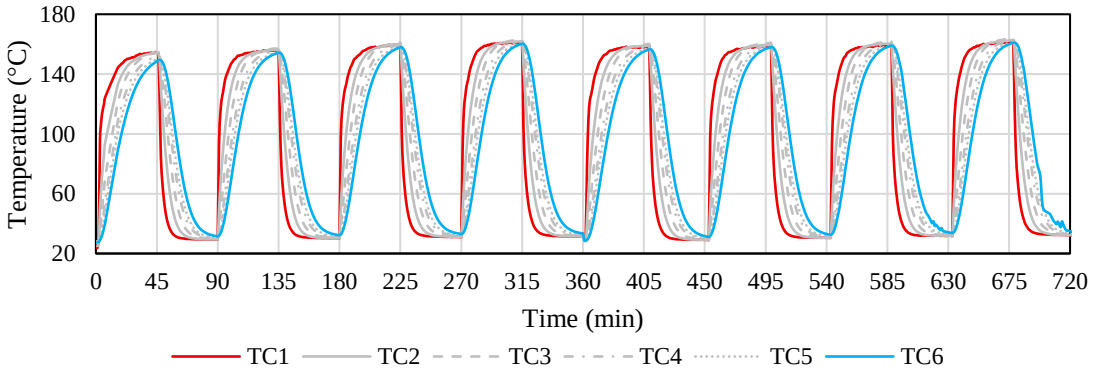
This section discusses the experimental results of the RA-PBTES system under repeated heating and cooling cycles. It examines temperature evolution, cyclic thermal response, thermocline development, and storage use. It then assesses the effects of particle size and material type on pressure drop and discharge to clarify thermo-hydraulic trade-offs. Lastly, the thermo-mechanical response of the packed bed and storage tank is analysed, focusing on particle rearrangement, deformation, and thermal ratcheting under cyclic operation. These findings provide an integrated view of the system's thermal, hydraulic, and structural behaviour.

3.1 Thermal Response of the RA-PBTES

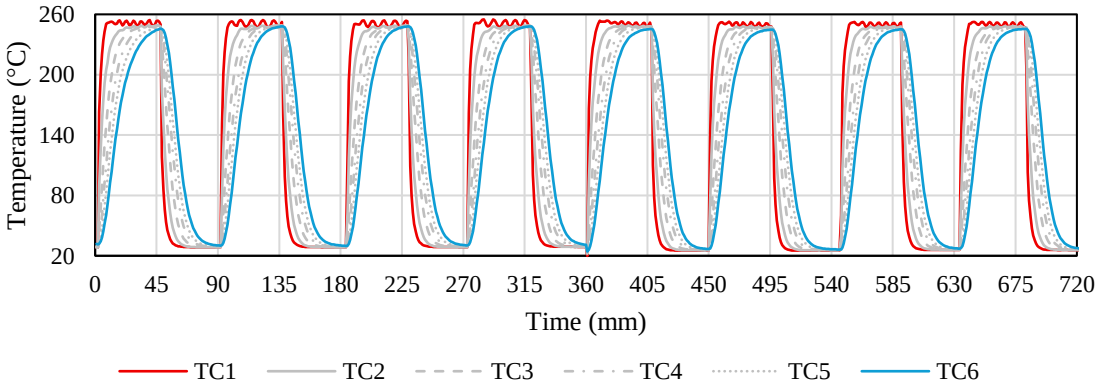
Figure 6 illustrates the temperature evolution at different axial locations (TC1–TC6) within the PBTES during repeated charging and discharging cycles. For all filler materials, clear thermal

stratification is observed, with temperature increasing sequentially from the inlet thermocouple (TC1) to the outlet thermocouple (TC6) during charging. During charging, the temperature decreases gradually from the bottom to the top of the bed, indicating thermal-front propagation through the packed particles. Compared with RA-a, the smaller particle size of RA-b increases the specific surface area for solid–fluid heat exchange, thereby enhancing the heat transfer between the packed particles and the heat transfer fluid. Compared with RA-a, RA-b and SFS show a more gradual axial temperature evolution during both charging and discharging. Although their smaller particle sizes provide a larger specific surface area for solid–fluid heat exchange, the denser packing of smaller particles also increases the solid fraction and volumetric thermal mass of the bed. Consequently, more energy is required to change the bed temperature in each time period, which slows overall propagation of the temperature front. The observed response therefore reflects the combined effects of particle size, packing density, porosity and material thermophysical properties rather than particle size alone [59].

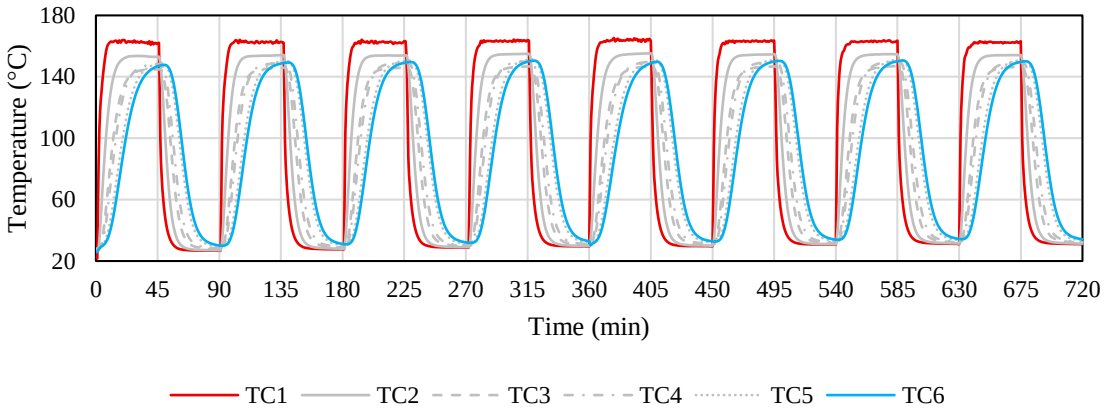
Although RA-b and SFS have relatively similar particle-size ranges, their temperature responses are not identical, indicating that material properties also play an important role. Differences in thermal conductivity, heat capacity, particle morphology and inter-particle contact conditions can influence both internal particle conduction and effective heat transfer through the packed bed. Therefore, the contrast between RA-b and SFS reflects the combined effects of material thermophysical properties and packing characteristics [60].



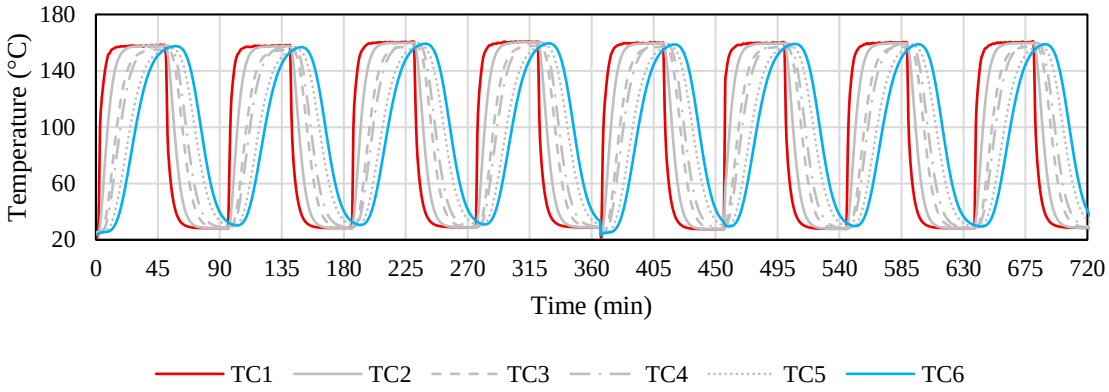
(a) RA-a1



(b) RA-a2



(c) RA-b

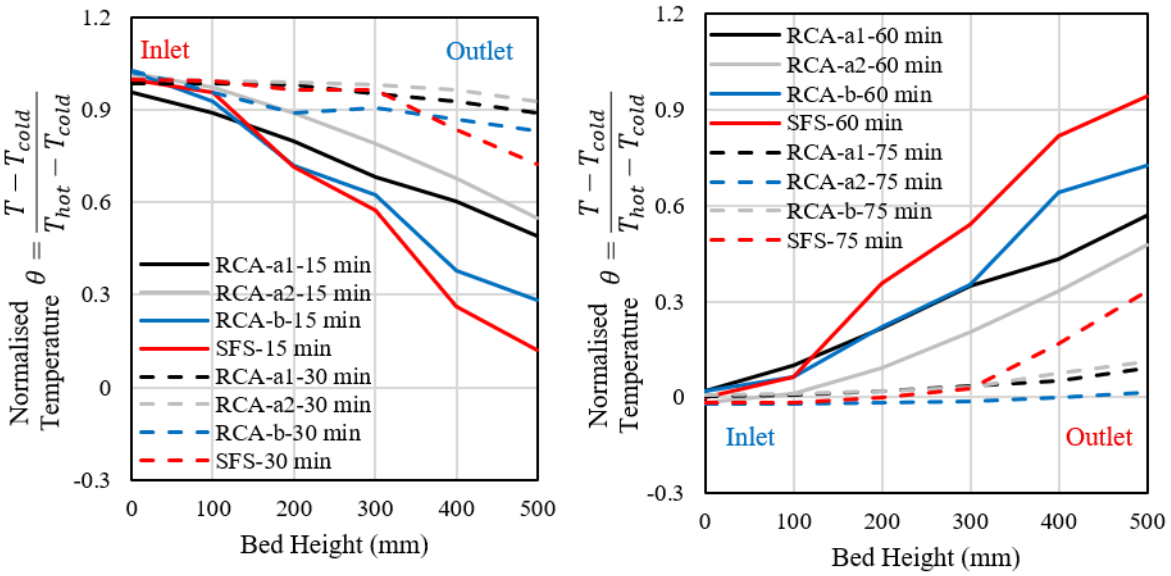


(d) SFS

Figure 6 Temperature distribution within the PBTES (TC1~6 ≡ from inlet to outlet) obtained from eight heating-cooling cycles

For comparison across the different test groups, the measured temperatures were normalised using the corresponding hot and cold reference temperatures T_{hot} (160 or 250 °C) and T_{cold} (30 C) defined in Table 2, as $\theta = (T\text{-}T_{cold}) / (T_{hot}\text{-}T_{cold})$. A normalised temperature θ of 0 therefore represents the cold reference state, while a value of 1 represents the hot reference state.

Figure 7 further compares the axial evolution of normalised temperature during Cycle No. 5. The 15 and 30 min profiles represent the charging stage, while the 60 and 75 min profiles correspond to 15 and 30 min after the start of discharging, respectively. During charging, the temperature decreases progressively from the inlet region at the bottom of the bed (i.e., hot inlet) towards the outlet (i.e., colder outlet), reflecting the upward propagation of the heat front. The RA-a cases retain relatively higher normalised temperatures over the upper part of the bed (outlet), whereas RA-b and SFS show a more pronounced decrease with path length (i.e., bed height), indicating a slower progression of the heated region. This behaviour is consistent with the denser packing and higher volumetric thermal mass of the smaller-particle beds, which require more energy to achieve a comparable temperature rise.

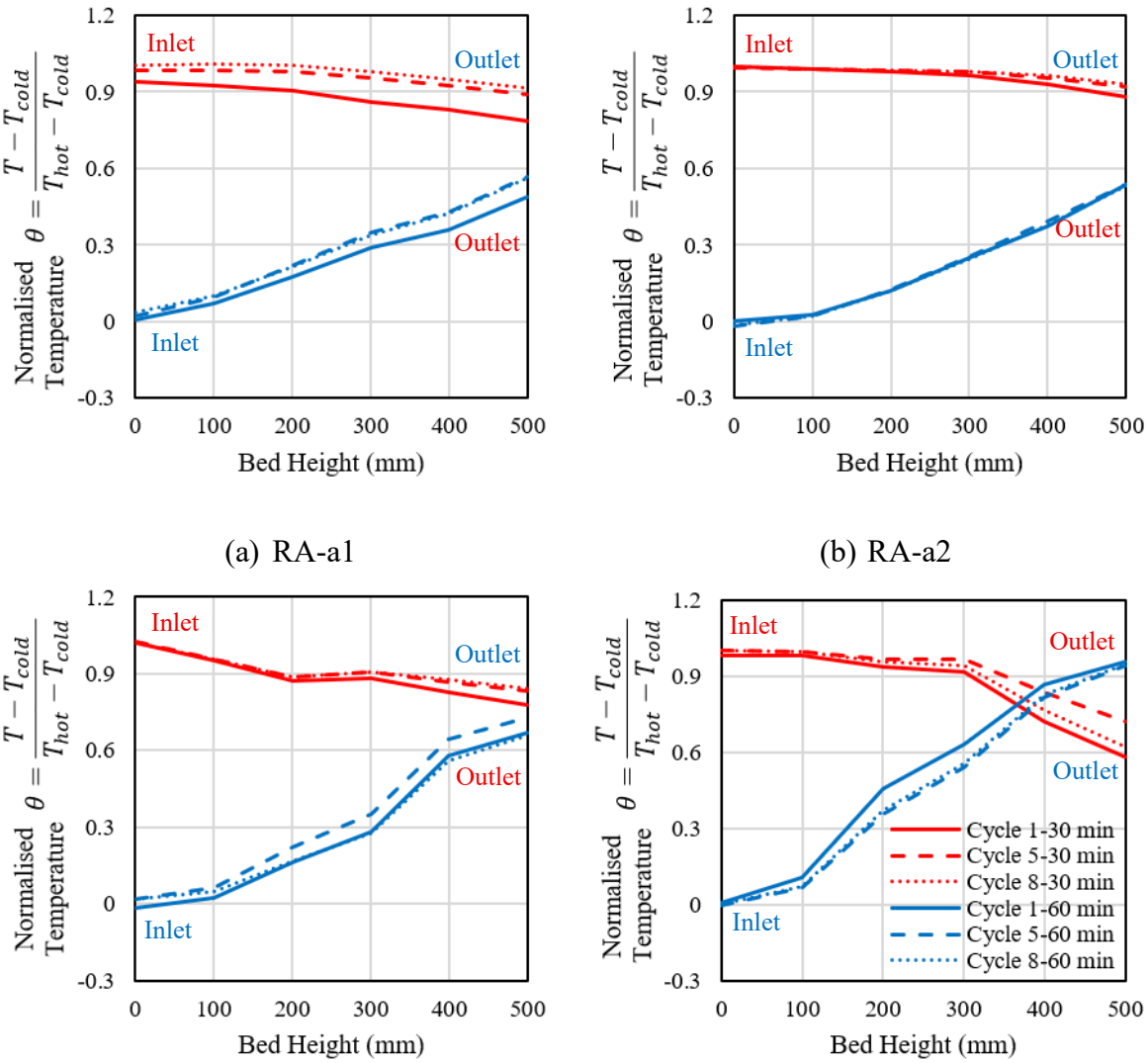


(a) Charging Stage (b) Discharging Stage

Figure 7 The normalised temperature change across the height of PBTES during the (a) charging and (b) discharging stages of Cycle 5

The axial temperature distributions at representative steady-state charging (30 min) and rapid discharging (60 min – only 15 min since thermal discharging starts) times for different cycles are compared in Figure 8 to evaluate the thermal stability of the PBTES system. The 30 and 60 min profiles were selected because they are symmetrically located 15 min before and after the 45 min charging–discharging transition. This avoids the instantaneous switching condition and provides representative late-charging and early-discharging states. Using the same relative operating times for Cycles 1, 5 and 8 further enables a consistent assessment of the evolution and repeatability of the axial thermal stratification, as commonly adopted in cyclic PBTES analyses [61].

For all three filler materials, the axial temperature profiles obtained in Cycles 1, 5 and 8 follow broadly similar trends, although some cycle-to-cycle variations are observed, particularly for RA-a1 and SFS. Such variations are not uncommon during repeated operation of packed-bed TES systems, where the temperature field may evolve over the initial cycles before approaching a recurrent thermal response. The literature has also reported cycle-to-cycle variation during the initial operation of packed-bed TES systems. Ortega-Fernández et al. [62] observed that the axial temperature distribution evolved during the first several charge–discharge cycles before becoming recurrent after approximately five to six cycles, at which point the system reached a stationary condition with reproducible thermal performance. In the present tests, RA-a2 shows the closest agreement between the selected cycles, whereas RA-a1 and SFS show larger variations. The axial temperature evolution remains comparable over repeated operation, indicating that the tested beds maintain a generally reproducible thermal response rather than an identical cycle-to-cycle temperature distribution.



(a) RA-a1 (b) RA-a2

(c) RA-b (d) SFS

Figure 8 Axial temperature distributions within the PBTES at representative charging (30 min) and discharging (60 min) times for Cycle 1/5/8: (a) RA-a1, (b) RA-a2, (c) RA-b, (d) SFS

3.2 Thermocline development and utilisation of bed capacity

Figure 9 presents the temporal evolution of the thermocline thickness during both the charging and discharging processes for three different filler materials in a typical charging and discharging cycle (Cycle 5). This comparison allows evaluation of how particle size and material properties influence the development of thermal stratification.

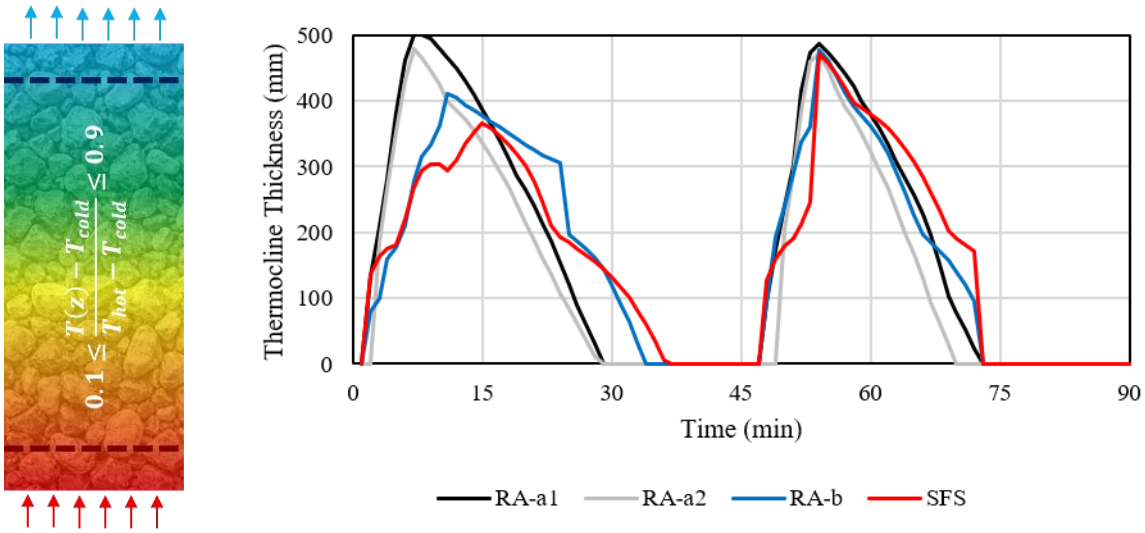


Figure 9 Typical thermocline thickness comparison of the PBTES (Cycle 5)

During the charging process (0–45 min), thermocline thickness initially increases rapidly as hot air enters the bed and heats the lower layers of packed particles. At this stage, the lower thermocouples rise rapidly while the upper part of the bed remains near the initial temperature, expanding the thermal transition zone. As the hot front continues to propagate upward, the thermocline reaches its maximum thickness, then gradually decreases as the entire bed approaches thermal equilibrium. Among the three filler materials, RA-a shows the most rapid expansion of thermocline thickness, reaching its peak earlier than the other materials. This behaviour is mainly attributed to its larger particle size (19~37.5 mm), which results in higher bed porosity and enhanced axial thermal dispersion. Consequently, the thermal front propagates more rapidly through the bed, resulting in a wider transition region during the early stages of charging. Once the hot region extends through most of the bed, the thermocline thickness decreases rapidly as the cold region diminishes.

In contrast, the SFS packed bed exhibits a relatively narrow, more gradual evolution of thermocline thickness. The smaller particle size of the steel slag provides a larger specific surface area for heat transfer between the solid and the heat-transfer fluid. This enhances the solid–fluid thermal exchange and reduces axial thermal dispersion, resulting in a sharper thermocline and improved thermal stratification. RA-b exhibits an intermediate behaviour between RA-a and SFS, reflecting the combined influence of particle size and material thermal properties. A similar trend is observed during the discharging stage (45–90 min), where the cold front propagates through the bed in the opposite direction. The thermocline thickness initially increases as the cold region develops, then gradually decreases as the bed approaches the initial temperature state. The consistent behaviour observed during both charging and discharging confirms the strong influence of particle size on thermocline formation and stability in PBTES. Compared with charging, the differences among the four cases become less pronounced during discharging. This may partly result from the combined effects of forced convective heat removal and heat loss to the surroundings, both of which contribute to the overall cooling of the packed bed. Previous studies have shown that wall and environmental heat losses can influence thermocline development and discharge behaviour in packed-bed

thermal storage systems [57, 63]. Under such conditions, differences arising from particle size and material properties may become less distinguishable.

3.3 Pressure-drop characteristics and particle-size effects

The pressure drop across the PBTES was monitored during repeated charging and discharging cycles to assess the system's flow resistance and hydraulic stability. Figure 10 shows the temporal variation in pressure drop across multiple operating cycles. In all cases, the pressure drop shows periodic fluctuations corresponding to cyclic heating and cooling of the storage bed. The consistent waveform over time indicates stable airflow and good system repeatability during long-term operation. Clear differences can be observed among the filler materials. The SFS packed bed shows the highest pressure drop, ranging from approximately 220–280 Pa, mainly because of its smaller particle size and reduced void fraction, which increases flow resistance. In contrast, RA-a shows the lowest pressure drop (around 90–130 Pa) because of its larger particle size and higher bed permeability. As presented in Table 1, the bed void fractions of RA-a and SFS are 58% and 48%, respectively, while RA-b exhibits an intermediate value of 52%. Although RA-b and SFS share the same nominal particle-size range (10–19 mm), identical size ranges do not necessarily result in identical packing structures. The void fraction of randomly packed beds is also influenced by particle morphology, size distribution, density, and packing arrangement [64, 65]. The different physical characteristics of RA and SFS therefore lead to distinct packing behaviours, which are reflected in their measured bed void fractions and corresponding pressure-drop responses.

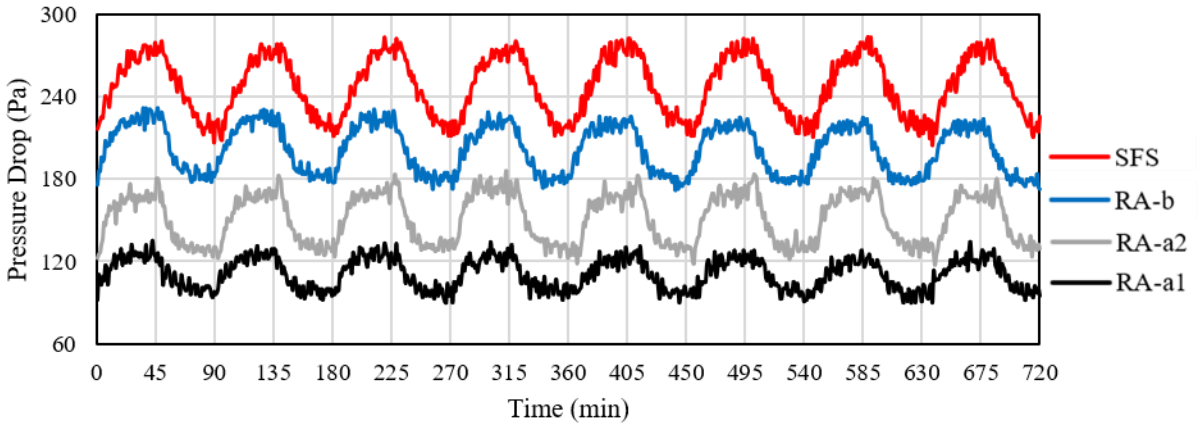


Figure 10 Pressure Drop of the PBTES

A comprehensive review of pressure drop correlations for packed beds (Table 3) was conducted by the recent study [66] systematically compared classical and modified Ergun-type equations for both spherical and non-spherical particles. Following the recommendations and comparative analysis presented in that review, the present study selected the Ergun equation [67] as a reference model and further evaluated the Tallmadge [68], Nemec & Levec [69], Harrison [70], and Özahi [71] correlations to assess the influence of particle irregularity on the pressure drop.

Table 3 Common friction factor equations for a packed bed [66]

Author	Friction factor (f)	Eq. No
Ergun [67]	$f = \frac{150(1-\varepsilon)}{Re_p} + 1.75$	(8)
Tallmadge [68]	$f = \frac{150}{Re_p} + \frac{4.2}{Re_p^{0.1666}}$	(9)
Harrison [70]	$f = \frac{119.8a}{Re_p} + \frac{4.63b}{Re_p^{0.1666}} \quad a = \left(1 + \frac{\pi D_p}{6L(1-\varepsilon)}\right)^2, b = 1 - \frac{\pi^2 D_p}{24L}$	(10)
Çarpinlioğlu & Özahi [71]	$f = \frac{139.57}{2}\left(\frac{D_p}{L}\right)^{0.5267} \frac{\varepsilon^{-0.3131}}{1-\varepsilon} Re_p^{-0.4733}$	(11)
Nemec & Levec [69]	$f = \frac{150}{\varphi^{3/2} Re_p} + \frac{1.75}{\varphi^{4/3}}$	(12)

*Note: All symbols used in this table are defined as follows:

Re_p is the particle Reynolds number defined as $Re_p = \frac{\rho_f u d_p}{\mu}$;
d_p is the particle diameter (m);
ρ_f is the fluid density (kg/m³);
u is the superficial velocity (m/s);
μ is the dynamic viscosity of the fluid (Pa·s);
φ is the particle sphericity;
D is the tank diameter (m);
L is the packed bed height (m);

The input parameters used in the pressure-drop correlations were determined consistently with the formulations summarised by Hassan and Hoffmann [66]. The representative particle diameter $d_p$was taken as the arithmetic mean of the upper and lower sieve sizes defining each particle-size range; the superficial velocity $u$was obtained from the measured airflow rate and tank cross-sectional area. The temperature-dependent density and dynamic viscosity of air were used for $\rho_f$and μ [72], respectively. For basic oxygen furnace slag, the mean φ of steel slag A distributed around 0.76 [73]; as for crushed RA, the average φ is around 0.72 [74].

Error! Reference source not found. compares the experimentally measured pressure drop with predictions from several packed-bed friction-factor correlations. For all three filler materials, the predicted pressure drops follow a consistent order: the Ergun model yields the lowest values, followed by the Tallmadge and Harrison correlations, while the Özahi and Nemec models predict relatively higher pressure drops. This trend is consistent with the increasing level of corrections these models introduce to account for non-spherical particle effects. For the RA-a bed, the measured pressure drop ranges from approximately 95 to 130 Pa and 130 to 180 Pa during charging. The Tallmadge and Harrison correlations agree most closely with the experimental results for RA-a1, while the Ergun model slightly underpredicts the pressure drop because it assumes spherical particles. When the particle size decreases and the packing density increases in the RA-b bed, the pressure drop increases significantly to around 180~220 Pa. In this case, the Tallmadge and Harrison models again provide reasonable predictions. The highest pressure drop is observed in the SFS bed, ranging from approximately 220 to 280 Pa. Consequently, the Nemec correlation, which explicitly accounts for particle sphericity effects, provides the closest prediction for the SFS case. The comparison

demonstrates that particle size, bed porosity, and particle morphology play critical roles in determining the hydraulic performance of packed-bed thermal energy storage systems. Models that account for non-sphericity, such as the Nemec correlation, are better suited to predicting highly irregular materials like SFS and RA.

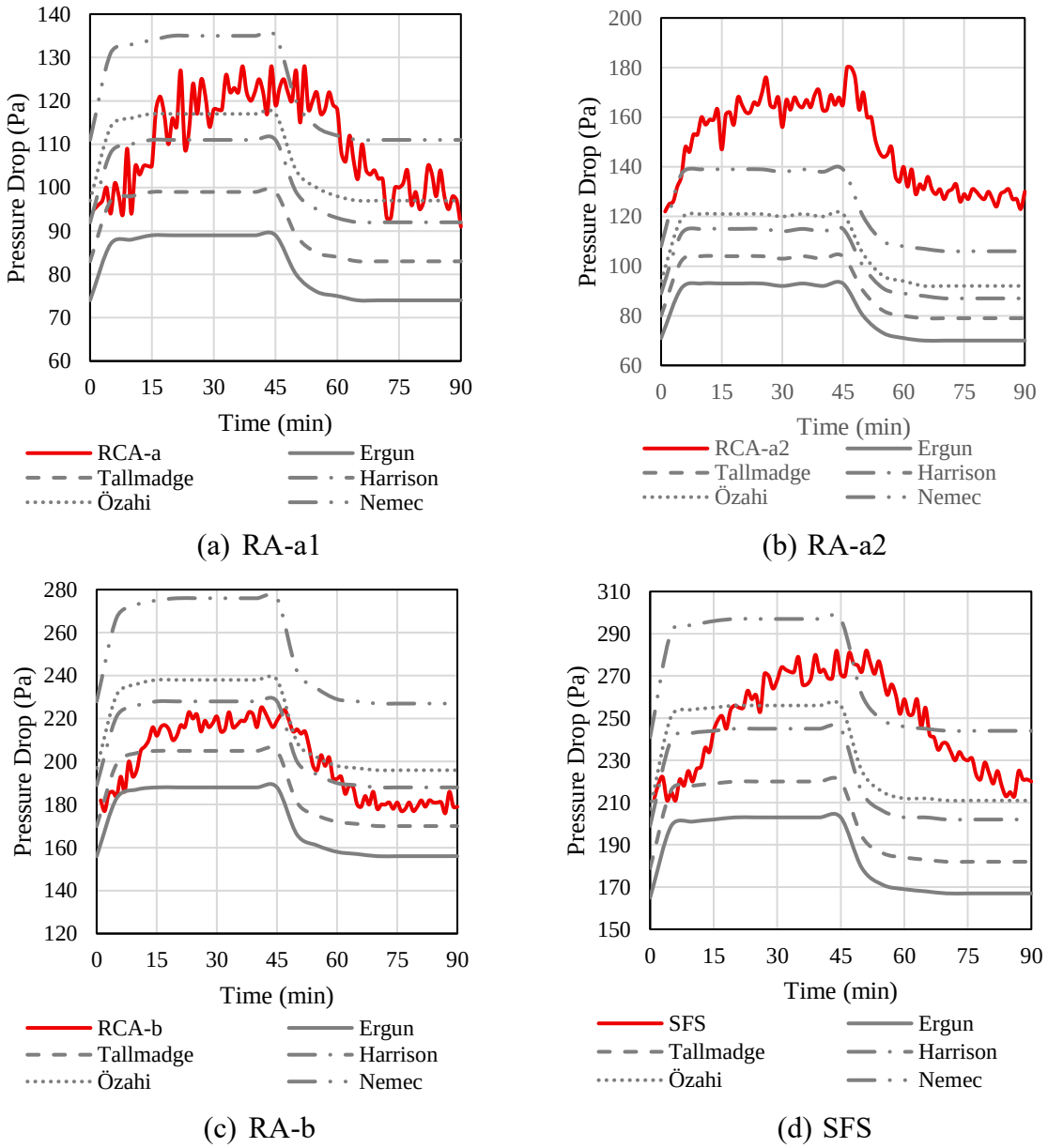


Figure 11 Comparison between experimentally measured (Cycle 5) and predicted pressure drops in the packed-bed TES (a) RA-a1, (b) RA-a2, (c) RA-b, (d) SFS using different friction factor correlations

3.4 Thermal Mechanical Behaviour of the Tank

To further evaluate the tank's thermal behaviour, the temperature evolution at the tank surface (TC7) and outer insulation layer (TC8) is monitored over multiple charging–discharging cycles, as shown in Figure 12. These measurements provide insight into heat transfer through the tank wall and the insulation's effectiveness under cyclic operation. The results show that the tank

surface temperature (TC7) closely follows the system's cyclic thermal behaviour, with peak temperatures during charging and rapid decreases during discharging. The temperature at the insulation layer (TC8) exhibits significantly lower amplitudes and delayed responses, indicating effective thermal resistance and reduced heat loss to the environment. Among the tested materials, the RA-based cases show thermal trends comparable to the SFS case, with slight differences in peak temperature and response time.

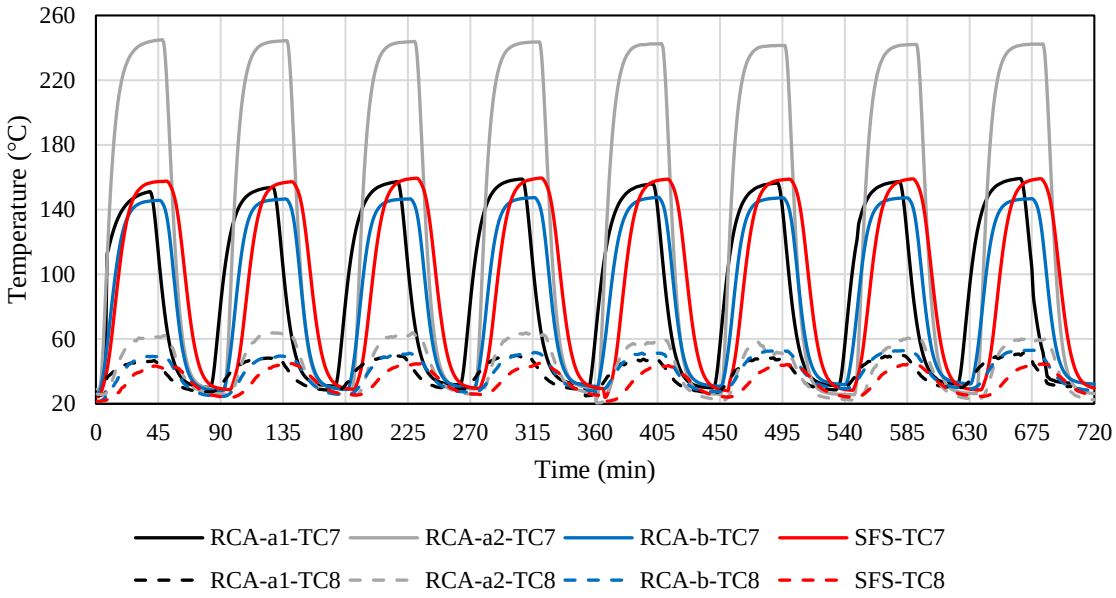
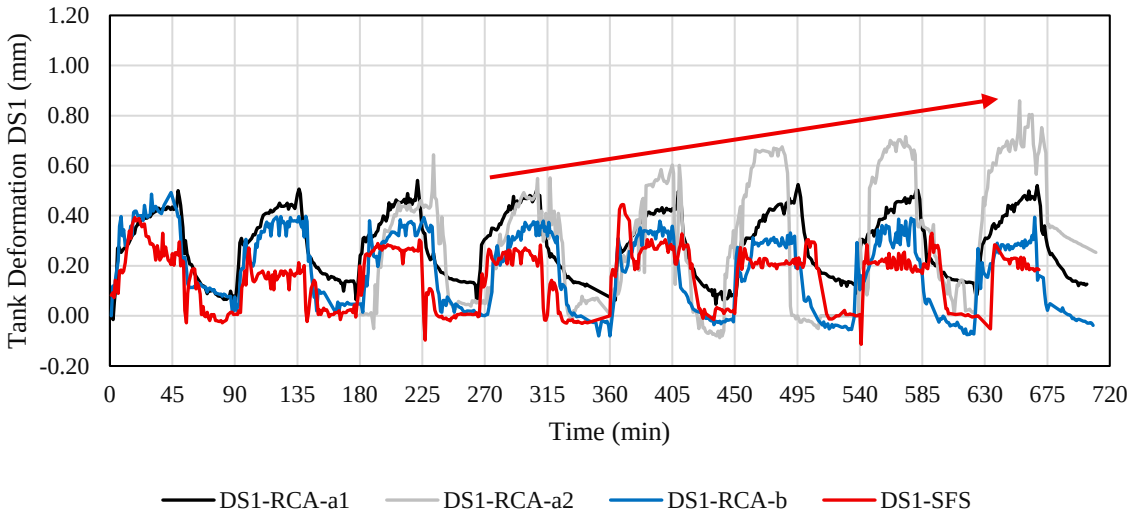
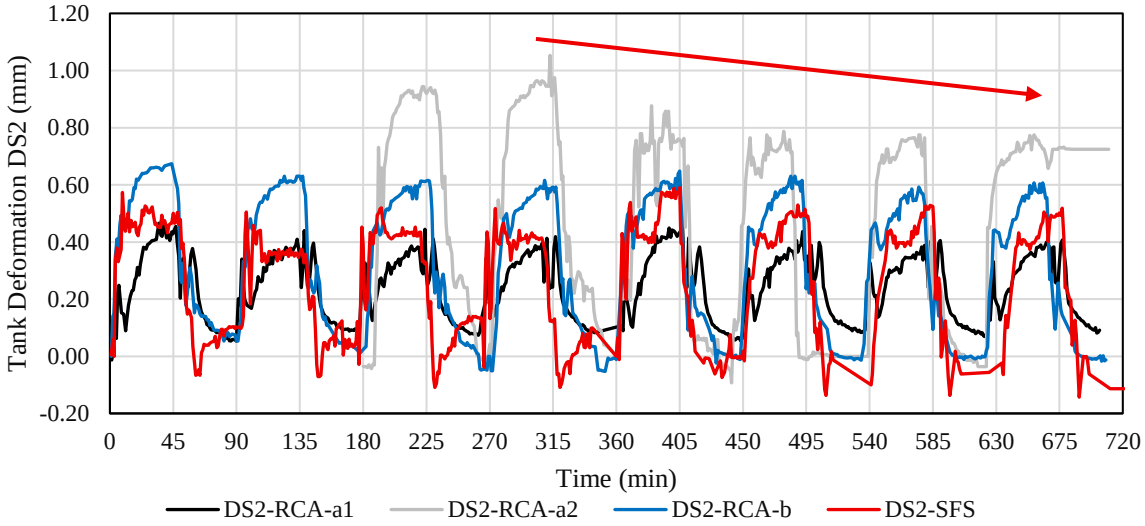


Figure 12 Comparison of temperature on the tank surface (TC7) and insulation (TC8)

Figure 13 shows tank-wall deformation measured at two different heights during multiple charging and discharging cycles. DS1 was installed at 125 mm near the lower region of the tank, while DS2 was located at 250 mm around the mid-height of the packed bed. In both locations, the deformation exhibits clear periodic behaviour corresponding to the system's cyclic heating and cooling. For the RA-a2 test, valid displacement data were available only from Cycle 3 onward because the laser displacement sensors experienced a temporary data-logging interruption during the first two cycles. Therefore, we present and discuss only the subsequently recorded cycles.



(a) DS1



(b) DS2

Figure 13 Deformation of the tank in the PBTES experiments

During charging, the tank wall expands as the bed temperature rises, leading to outward deformation. During discharging, the temperature decreases, and the tank gradually contracts. This cyclic expansion and contraction are consistently observed throughout the repeated cycles. The magnitude of deformation differs between the two measurement locations. In general, the deformation measured at DS2 (mid-height) is slightly larger than at DS1 for some materials, suggesting that thermal expansion of the tank wall and internal pressure generated by the packed particles are not uniformly distributed along the tank height. The differences among filler materials are also evident. The RA-a1 bed tends to produce relatively larger deformation in the lower section (DS1), whereas the RA-b bed shows larger deformation near the mid-height (DS2). The different deformation profiles of RA-a1 and RA-b may reflect differences in granular stress transmission arising from their particle sizes and packing structures. Previous studies of packed-bed thermocline tanks have shown that particle–wall interactions and downward particle rearrangement during thermal cycling can modify the radial stress distribution along the tank height, thereby producing non-uniform wall deformation [75, 76].

Particle size has also been shown to influence the magnitude and distribution of lateral wall pressure in confined granular beds [77]. Therefore, the smaller and more densely packed RA-b particles may redistribute lateral loading differently from the coarser RA-a1 bed, contributing to the observed difference in the location of maximum tank-wall deformation.

While most cases show stable and reversible deformation, the RA-a2 case at high temperature shows progressive deformation accumulation; the deformation response became progressively asymmetric at higher operating temperatures. The lower sensor (DS1) showed an increasing radial displacement over successive cycles, whereas the mid-height sensor (DS2) exhibited a decreasing trend. This behaviour likely reflects irreversible particle rearrangement and downward migration within the packed bed, which progressively increased local packing and lateral loading in the lower section while reducing confinement around the mid-height region. In contrast, RA-b and SFS cases exhibit more stable deformation amplitudes over cycles, highlighting the influence of particle size distribution and morphology on mechanical stability. The SFS bed exhibits more irregular deformation patterns, which may be associated with the higher angularity and stronger interlocking of steel slag particles.

4 Analysis of a 1 MWh RA-PBTES module

This section extends the laboratory-scale observations to a larger engineering context through analytical modelling and system-level assessment. A one-dimensional transient heat-transfer model based on the Schumann formulation is first developed and solved using the finite difference method, and its predictions are validated against the experimental temperature measurements reported in Section 3. The validated model is then applied to a 1 MWh RA-PBTES module to evaluate thermal performance, thermocline behaviour, fan energy demand, and net energy output under representative operating conditions. MWh-scale thermal storage is relevant to both district-heating and industrial process-heat applications. For residential heating, reported average annual heat demand across several European district-heating markets ranges from approximately 11.4 to 18.6 MWh per household, including space heating and domestic hot water [78]. On an equivalent energy basis, a 1 MWh storage unit therefore represents approximately 20–32 days of the average heat demand of one household, or roughly one day of average heat demand for 20–30 households. At the industrial scale, the Hardwick Meatworks project in Victoria employs a 1 MW-class heat-pump system for process-hot-water production, with an operating thermal output of approximately 1.09–1.27 MW and supplying around 61% of the site hot-water demand [79]. MWh-scale packed-bed storage has also been demonstrated directly for district heating, including a 2.0 MWh air–rock packed-bed system reported by Jia et al. [80]. These examples indicate that the 1 MWh capacity considered here should be interpreted as a representative modular storage unit rather than as the total thermal requirement of a large community. Larger thermal demands could be accommodated by increasing module size or operating multiple modules in parallel. Finally, the implications of large-scale RA utilisation are discussed in terms of material demand, cost, environmental

considerations, and the potential integration of thermal storage with downstream aggregate upgrading and recovery.

4.1 Finite Difference Method with Schumann's Model

Assessing the performance of large-scale TES systems requires reliable predictions of their thermal behaviour under realistic operating conditions. Modelling approaches are commonly employed to extrapolate the thermal performance of experimentally validated systems to larger storage capacities. A simplified one-dimensional PBTES thermal model is developed in MATLAB using a finite-difference method (FDM) [40] and Schumann's model [41] to describe transient heat-transfer behaviour within the storage system. The thermal behaviour of the RA-a PBTES system was modelled based on the fundamental principles of energy conservation in porous media. Heat losses through the tank wall are accounted for by an overall heat transfer coefficient determined from the thermal resistance of the insulation layer and the external convective resistance. The model is expressed by the following equations:

Fluid Phase:
$$\varepsilon\rho_f c_{p,f}\frac{\partial T_f}{\partial t} + \rho_f c_{p,f} u\frac{\partial T_f}{\partial z} = ha\left(T_s - T_f\right) - h_l a_l (T_f - T_{amb}) \quad (14)$$

Solid Phase:
$$(1-\varepsilon)\rho_s c_{p,s}\frac{\partial T_s}{\partial t} = ha\left(T_f - T_s\right) \quad (15)$$

$$h = \frac{Nu\cdot k_f}{d_p} \quad (16)$$

Interphase heat transfer
$$Nu = 2 + 1.1Re^{0.6}Pr^{1/3} \quad (17)$$

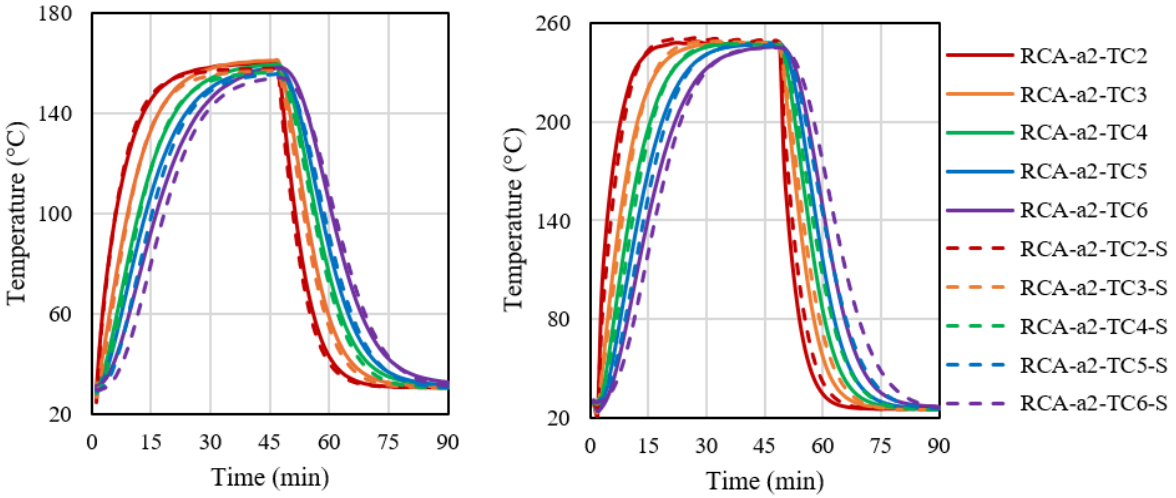
$$Re = \frac{\rho_f u d_p}{\mu}, Pr = \frac{c_{p,f}\mu}{k_f} \quad (18)$$

Specific surface area
$$a = \frac{6(1-\varepsilon)}{\varphi d_p}, a_l = \frac{4}{D} \quad (19)$$

where z is the axial coordinate. h is the interphase heat transfer coefficient (W/m^2·K), and a is the specific surface area of particles (m^{-1}). a_l is the specific surface area of the cylindrical tank (m^{-1}). k_f is the fluid thermal conductivity (W/m·K), and μ is the fluid dynamic viscosity (Pa·s). The properties of the air are temperature-dependent [81]. u is the superficial velocity (0.6 m/s). The heat loss to the environment is evaluated using a thermal resistance network, considering heat conduction through the insulation layer and natural convection to ambient air ($T_{amb} = 26\ °C$). The overall heat transfer coefficient is expressed as:

$$h_l = \frac{1}{\frac{L_{ins}}{k_{ins}} + \frac{1}{h_{air}}} \quad (20)$$

where L_{ins} and k_{ins} denote the thickness (0.03 m) and thermal conductivity (0.04 W/m·K) of the insulation layer, respectively, and h_{air} is the external convective heat transfer coefficient (20 W/m^2·K) [82]. The internal convective resistance is neglected because of the relatively high heat-transfer rate within the packed bed. The resulting heat-loss term is incorporated into the fluid energy equation as a volumetric sink.



(a) RA-a1 (b) RA-a2

Figure 14 Comparison between experimental measurements (Cycle 1 – solid line) and model predictions (dashed line, -S suffix_) of the temperature evolution at different thermocouple locations: (a) RA-a1, (b) RA-a2

Figure 14 compares the temperature evolution at different thermocouple locations from the experiment and the simulation based on Schumann's model. The simulated temperature evolution agrees well with the experimental measurements at all thermocouple locations. Schumann's model captures the general thermal response of the packed bed during both charging and discharging. Minor deviations in the thermocline propagation speed (as shown in the TC4 and TC6 temperature development) may be attributed to flow maldistribution and heterogeneity in particle packing in the experimental system. The discrepancy between the experimental result and the modelling prediction is also higher for the RA-a2 model than for the RA-a1 model. The good agreement indicates that Schumann's model is suitable for the present RA-PBTES. Although the model neglects intra-particle temperature gradients [83], its agreement with the experiments suggests that this simplification remains reasonable for the irregular RA particles under the present operating conditions.

4.2 Thermal and Net Energy Performance

Using the validated Schumann's model, the thermal and net energy performance of a 1MWh RA-PBTES is investigated in this section. For a temperature range of 30–250 °C, the 1 MWh RA-PBTES system requires approximately 18 t of filler material, corresponding to a bed volume of 12 m³. Considering thermocline effects, the practical tank volume is estimated at 15 m³, achievable with a cylindrical tank 2.2 m in diameter and 5.5 m in height. The fan power

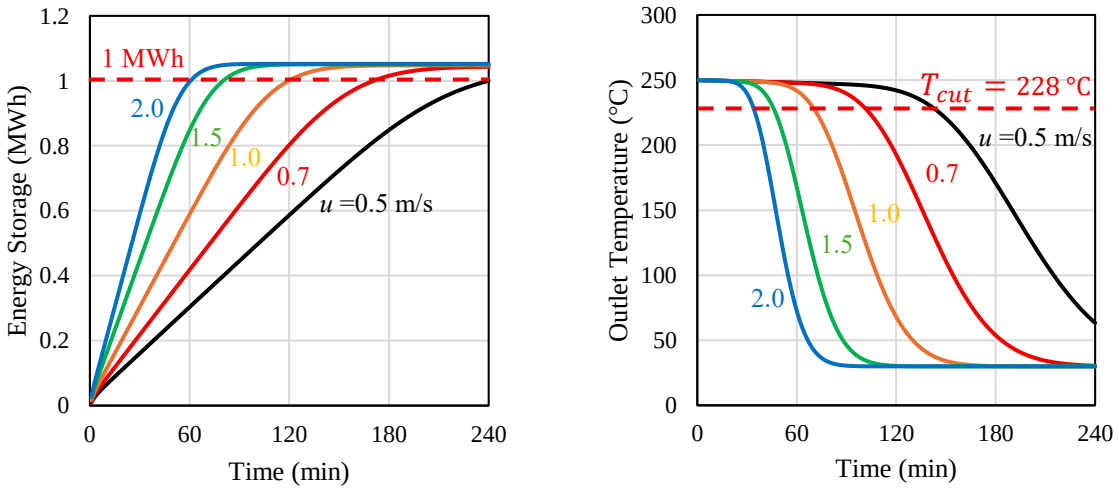
required could be estimated based on the measured pressure drop across the packed bed and the corresponding airflow rate [84]:

$$P_{fan} = \frac{\Delta P \cdot \dot{V}}{\eta_{fan}} \tag{21}$$

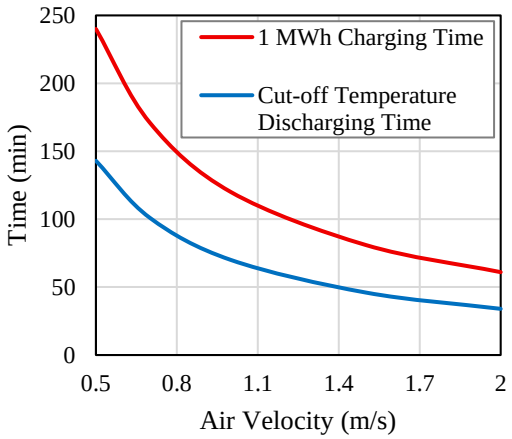
$$\dot{V} = u \cdot A \tag{22}$$

where P_{fan} is the fan power (W), $\dot{V}$ is the volumetric flow rate (m³/s), and η_{fan} is the fan efficiency (0.88 for comparison). A is the cross-sectional area of the packed bed (m²). Nemec & Levec [69] correlation, which shows high accuracy in predicting pressure drop in Section 3.3, is used for pressure-drop comparison.

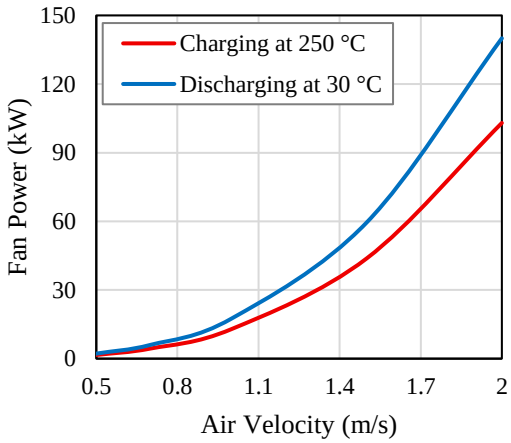
Figure 15 presents the performance of the RA PBTES system under different airflow velocities. The "instantaneous" stored energy was obtained from the Schumann-model solid-temperature distribution by integrating the sensible heat content of the filler over the packed-bed volume relative to the cold reference temperature (Eq. (1)). As shown in Figure 15 (a), increasing the air velocity significantly accelerates the charging process, with the stored energy approaching its maximum value much faster at higher velocities. For instance, at 2.0 m/s, the system reaches near-full capacity within about one hour, whereas at 0.5 m/s, charging is considerably slower and remains incomplete even after extended operation. A similar trend is observed during discharging, as illustrated in Figure 15 (b). Higher airflow velocities lead to a more rapid decline in outlet temperature, indicating faster heat extraction from the packed bed. This behaviour reflects enhanced convective heat transfer between the air and solid filler at higher Reynolds numbers.



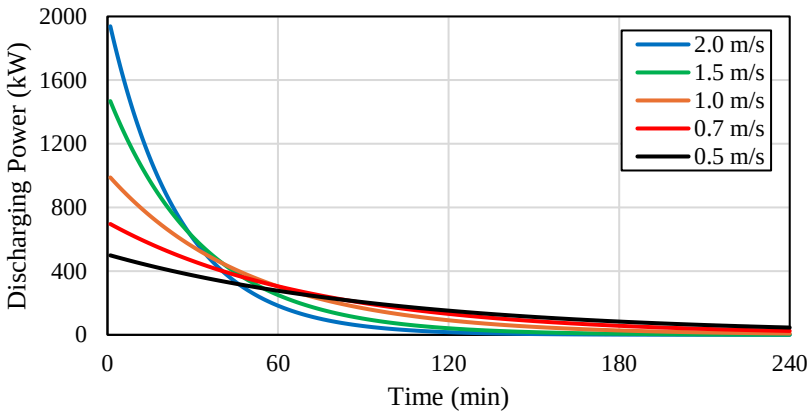
(a) Energy Storage (Charging, 250 °C) (b) Outlet Temperature (Discharging, 30 °C)



(c) Charging/Discharging Time



(d) Fan Power



(e) Discharging Power

Figure 15 Scale-up RA PBTES Module Behaviour Analysis

The trade-off between thermal performance and operational cost is clearly highlighted in Figure 15(c) and (d). Increasing airflow velocity substantially reduces both charging and discharging times; however, this improvement comes at the expense of a sharp increase in fan power consumption. Notably, fan power grows nonlinearly with velocity, resulting in disproportionately high energy consumption above 1.0 m/s. These results indicate that while high airflow velocities improve thermal response and reduce operation time, they significantly increase parasitic energy consumption. Therefore, an optimal operating range exists, typically between 0.5 and 0.8 m/s, where a balance can be achieved between efficient heat transfer and acceptable pumping energy requirements. This highlights the importance of integrated thermo-hydraulic optimisation in designing large-scale PBTES systems. The discharging power in Figure 15(e) shows that increasing airflow velocity significantly increases peak discharging power because of the higher mass flow rate. For example, at 2.0 m/s, the initial discharging power exceeds 1.9 MW, compared to approximately 0.5 MW at 0.5 m/s. However, the higher flow rate also accelerates the thermal depletion of the packed bed, leading to a rapid drop in outlet temperature and a shorter effective discharge duration. In contrast, lower flow rates provide more sustained heat release with reduced peak power. This highlights a fundamental trade-off between power output and discharge duration in PBTES systems.

4.3 Circular Material Utilisation, Cost and Environmental Implications

Unlike conventional TES systems that rely on inert or non-recyclable filler materials, using RA introduces an additional lifecycle dimension. After repeated thermal cycles, the filler material can be processed by grinding and sieving in the thermo-mechanical recovery (TMR) process to recover reusable aggregates and cementitious powder [25], thereby enabling a closed-loop material pathway. Table 4 presents a comparative evaluation of different filler materials for PBTES. While materials such as recycled ceramic achieve high energy densities due to their wide operating temperature ranges, their prohibitively high costs significantly limit practical application. In contrast, steel slag and limestone offer a more balanced performance, combining moderate-to-high energy densities with relatively low material costs. Notably, RA demonstrates a unique advantage among all materials considered. Although its initial procurement cost is approximately 100 AUD/m^3 [85], RA undergoes thermal treatment during TES operation, which can facilitate removing or weakening attached mortar. This process enables reprocessing and reuse as high-quality aggregate after its service life in the TES system [45]. As a result, RA has a potential residual or recovery value that can offset or even exceed its initial cost. This results in a negative net material cost from a lifecycle perspective. Compared with other materials that are consumed or degraded over time, this circular utilisation pathway gives RA a significant economic advantage.

Table 4 A comparison of filler materials used in the PBTES and the cost per kWh

Filler Material	Demolition Waste [20]	Steel Slag [25]	Limestone [86]	Recycled Ceramic [87]	Stearic Acid (PCM) [88]	RA
T (°C)	290~565	20~300	300~585	20~1000	30~68	30~250
d_P/D	0.015	0.046~0.091	0.005	0.144	0.150	0.095~0.188
ε	22%	42%	33%	43%	56%	58%
HTF	Molten Salt	Air	Solar Salt	Air	Air	Air
Q'''_{max} (kWh/m^3)	266	154	231	352	26.5	51.7
Cost (AUD/m^3)	6.3	44.0 [89]	36.96	2400.0 [27]	2000.0 [90]	-5.0
Cost per kWh (AUD/kWh)	0.02	0.29	0.16	6.82	75.50	-0.10

*d_P/D denotes the ratio of particle diameter to tank diameter.

According to the life cycle assessment of the TMR [43], the total energy consumption of ball milling and sieve shaker steps is approximately 20 kWh/t of RA. The results indicate that the proposed TMR process emits approximately 106 kg CO_2/t, whereas conventional cement production emits approximately 953 kg CO_2/t. The operating temperature of the current PBTES system (250 °C) is lower than that typically required for RA thermal activation (600 °C).

691 However, the stored thermal energy can be repeatedly utilised over multiple charging–
692 discharging cycles, resulting in a cumulative thermal input comparable to that of high-
693 temperature short-duration treatments. A simplified energy-equivalence analysis suggests that
694 approximately 6–8 cycles may provide a total energy input like that required for conventional
695 thermal activation (1 425 MJ/t). Nevertheless, the underlying mechanisms differ from those of
696 conventional high-temperature treatment. High-temperature exposure can directly promote
697 dehydration and weakening of the mortar–aggregate interface, whereas repeated moderate-
698 temperature cycling is more likely to induce progressive damage through differential thermal
699 expansion, microcracking, and repeated interfacial stress. A conceptually similar cumulative-
700 damage mechanism has been reported for freeze–thaw treatment of recycled aggregate, where
701 repeated cycles progressively weaken and detach adhered mortar from the original aggregate
702 surface [91, 92]. Such studies demonstrate that repeated cyclic exposure, even when individual
703 cycles are insufficient to cause extensive material degradation, can progressively alter the
704 integrity of attached mortar. The present PBTES cycling may therefore provide a gradual
705 thermal pre-conditioning effect that facilitates subsequent mechanical processing of RA rather
706 than directly replacing conventional high-temperature treatment. This indicates that the
707 proposed approach represents a low-temperature, multi-cycle alternative to conventional high-
708 temperature processing, potentially improving energy utilisation efficiency.

709 5 Conclusions and Outlook

710 The key lessons from this experimental and numerical study, along with potential directions
711 for future work, are summarised below.

712 5.1 Conclusions

713 This study demonstrates the technical feasibility and sustainability potential of using recycled
714 aggregate (RA) as a filler material in packed-bed thermal energy storage (PBTES) systems.
715 Conclusions have been summarised as follows:

716 1. Experimental results show that the RA packed bed can achieve stable thermal stratification
717 within the operating temperature range of approximately 30–250 °C. The system shows
718 clear thermocline formation and predictable temperature evolution during both charging
719 and discharging. The packed-bed pressure drop is strongly influenced by particle size and
720 morphology. For the RA beds, the pressure drop ranges from approximately 130~180 Pa
721 (RA-a, 160 °C/250 °C) and increases to 220 Pa (RA-b) due to reduced particle size and
722 lower porosity. The SFS bed exhibits the highest pressure drop, ranging from 220 to 280 Pa,
723 attributed to its greater angularity and surface roughness. The Nemec correlation performs
724 best for pressure-drop prediction, highlighting the importance of accounting for particle
725 shape effects in predicting hydraulic behaviour.

726 2. Cyclic deformation of the tank is observed under repeated thermal loading, with the RA-
727 a2 case at 250 °C exhibiting progressive deformation accumulation (thermal ratcheting),
728 while other cases remain largely stable. This highlights the importance of particle

characteristics and operating temperature in governing the long-term structural stability of packed-bed systems.

3. The one-dimensional Schumann-based model showed good agreement with experimental data in predicting temperature evolution and thermocline movement. The validated model provides an efficient tool for scaling analysis, enabling the prediction of system performance and pumping energy requirements for a 1MWh RA-PBTES. The volumetric heat storage capacity of RA is estimated at 51.7 kWh/m³ at a target temperature of 250 °C, demonstrating competitive performance among low-cost sensible heat storage materials. RA offers significant advantages due to its low cost, wide availability, and contribution to the valorisation of construction and demolition waste. Compared to alternative materials, RA offers a pathway whereby, after thermal cycling, it can be further processed and reused as a construction material. The stored thermal energy can potentially offset part of the processing energy demand, enhancing overall system sustainability.

5.2 Outlook

Future research should first establish the long-term thermal and thermo-mechanical stability of recycled aggregate under repeated charging–discharging conditions. The present study demonstrates short-term cyclic repeatability, whereas substantially extended testing is required to quantify progressive particle breakage, strength degradation, mortar detachment, interfacial transition zone deterioration, and changes in packed-bed structure. These effects may alter heat-transfer efficiency, pressure drop, dust generation, and overall system reliability over prolonged operation. Attention should also be given to the influence of operating temperature, thermal-cycle duration, heating and cooling rates, moisture content, and RA source variability.

At the system level, further work should assess how RA-based packed-bed thermal energy storage can be integrated with renewable heat, industrial waste-heat recovery, and thermal-mechanical recycling processes. Such integration could enable cascading utilisation of construction and demolition waste, in which RA is first employed as a thermal storage medium before entering subsequent material-recovery or recycling pathways. Larger-scale validation, energy-flow optimisation, and techno-economic assessment are therefore required to determine the operating conditions under which the thermal benefit of RA outweighs pressure-loss-related auxiliary energy demand. A comprehensive life-cycle assessment should also quantify the effects of material processing, transportation distance, avoided use of virgin material, operational energy consumption, and end-of-life reuse.

More fundamental studies are required to clarify the coupled thermal, mechanical, and fluid-dynamic mechanisms governing RA behaviour in packed beds. It remains unclear whether increased airflow velocity or rapid thermal cycling could induce internal stress accumulation and particle damage through short-duration exposure to elevated convective heat-transfer rates. Addressing these questions will require controlled experiments combined with multi-physics modelling that can resolve particle-scale heat transfer, airflow distribution, contact mechanics, and damage evolution. Such work would support the development of predictive design tools

and enable more reliable optimisation of RA particle size, bed configuration, and operating conditions for large-scale packed-bed thermal energy storage.

Declaration of competing interests

The authors declare no known competing financial interests or personal relationships that could have appeared to influence the work reported in this paper.

Acknowledgement

This research is supported by the Australian Research Council Discovery Early Career Researcher Award (ARC DE240100548) and the Program of China Scholarship Council (CSC NO. 202106090007). Support from the University of Melbourne's Research Computing Services and from the ARC DP210100433 is also greatly acknowledged.

Reference

[1] E. t. E. Department of Climate Change and Water, "Renewable energy." [Online]. Available: https://www.dcceew.gov.au/energy/renewable.

[2] Z. Ding, W. Wu, and M. Leung, "Advanced/hybrid thermal energy storage technology: material, cycle, system and perspective," *Renewable and Sustainable Energy Reviews,* vol. 145, p. 111088, 2021/07/01/ 2021, doi: https://doi.org/10.1016/j.rser.2021.111088.

[3] J. Vera, O. Sanmartí, S. Torras, and C. D. Pérez-Segarra, "Optimizing structured thermocline performance using a 3D+1D advanced model," *Energy Conversion and Management: X,* vol. 28, p. 101252, 2025/10/01/ 2025, doi: https://doi.org/10.1016/j.ecmx.2025.101252.

[4] D. Enescu, G. Chicco, R. Porumb, and G. Seritan, "Thermal energy storage for grid applications: Current status and emerging trends," *Energies,* vol. 13, no. 2, p. 340, 2020.

[5] I. Sarbu and C. Sebarchievici, "A comprehensive review of thermal energy storage," *Sustainability,* vol. 10, no. 1, p. 191, 2018.

[6] K. Vigneshwaran, G. Singh Sodhi, P. Muthukumar, and S. Subbiah, "Concrete based high temperature thermal energy storage system: Experimental and numerical studies," *Energy Conversion and Management,* vol. 198, p. 111905, 2019/10/15/ 2019, doi: https://doi.org/10.1016/j.enconman.2019.111905.

[7] A. Gil *et al.*, "State of the art on high temperature thermal energy storage for power generation. Part 1—Concepts, materials and modellization," *Renewable and sustainable energy reviews,* vol. 14, no. 1, pp. 31-55, 2010.

[8] H. Benoit, L. Spreafico, D. Gauthier, and G. Flamant, "Review of heat transfer fluids in tube-receivers used in concentrating solar thermal systems: Properties and heat transfer coefficients," *Renewable and Sustainable Energy Reviews,* vol. 55, pp. 298-315, 2016/03/01/ 2016, doi: https://doi.org/10.1016/j.rser.2015.10.059.

[9] N. Georgousis, J. Diriken, M. Speetjens, and C. Rindt, "Comprehensive review on packed-bed sensible heat storage systems," *Journal of Energy Storage,* vol. 121, p. 116516, 2025/06/15/ 2025, doi: https://doi.org/10.1016/j.est.2025.116516.

[10] Z. Han, B. Su, X. Zeng, and Z. Xu, "Dynamic performance analysis of thermocline packed bed thermal energy storage system with hybrid structure," *Energy Conversion and Management,* vol. 349, p. 120832, 2026/02/01/ 2026, doi: https://doi.org/10.1016/j.enconman.2025.120832.
[11] A. Gautam and R. P. Saini, "A review on sensible heat based packed bed solar thermal energy storage system for low temperature applications," *Solar Energy,* vol. 207, pp. 937-956, 2020/09/01/ 2020, doi: https://doi.org/10.1016/j.solener.2020.07.027.
[12] M. I. Khan, F. Asfand, and S. G. Al-Ghamdi, "Progress in research and technological advancements of thermal energy storage systems for concentrated solar power," *Journal of Energy Storage,* vol. 55, p. 105860, 2022.
[13] M. T. Ameen, Z. Ma, A. Smallbone, R. Norman, and A. P. Roskilly, "Experimental study and analysis of a novel layered packed-bed for thermal energy storage applications: A proof of concept," *Energy Conversion and Management,* vol. 277, p. 116648, 2023/02/01/ 2023, doi: https://doi.org/10.1016/j.enconman.2022.116648.
[14] C. A. Vielma, M. Majó, A. Calderón, A. Svobodova-Sedlackova, A. I. Fernández, and C. Barreneche, "Life cycle assessment of a conventional thermal energy storage system versus an alternative steel slag-based system for concentrating solar power plants," *Journal of Energy Storage,* vol. 145, p. 119843, 2026/02/01/ 2026, doi: https://doi.org/10.1016/j.est.2025.119843.
[15] P. Tatsidjodoung, N. Le Pierrès, and L. Luo, "A review of potential materials for thermal energy storage in building applications," *Renewable and Sustainable Energy Reviews,* vol. 18, pp. 327-349, 2013/02/01/ 2013, doi: https://doi.org/10.1016/j.rser.2012.10.025.
[16] I. Ortega-Fernández, N. Calvet, A. Gil, J. Rodríguez-Aseguinolaza, A. Faik, and B. D'Aguanno, "Thermophysical characterization of a by-product from the steel industry to be used as a sustainable and low-cost thermal energy storage material," *Energy,* vol. 89, pp. 601-609, 2015/09/01/ 2015, doi: https://doi.org/10.1016/j.energy.2015.05.153.
[17] Y. Rong, S. Y. Huang, and H. Zhou, "Experimental study on storage performance of packed bed solar thermal energy storage system using steel slag," *Journal of Energy Storage,* vol. 78, p. 110042, 2024/02/01/ 2024, doi: https://doi.org/10.1016/j.est.2023.110042.
[18] E. Alonso, E. Rojas, R. Bayón, M. Rodríguez, and A. Ávila-Marín, "Experimental comparison of tailored and natural solid fillers for high-temperature air-packed-bed thermal energy storage," *Case Studies in Thermal Engineering,* vol. 75, p. 107222, 2025/11/01/ 2025, doi: https://doi.org/10.1016/j.csite.2025.107222.
[19] A. de Bortoli, "Understanding the environmental impacts of virgin aggregates: Critical literature review and primary comprehensive life cycle assessments," *Journal of Cleaner Production,* vol. 415, p. 137629, 2023/08/20/ 2023, doi: https://doi.org/10.1016/j.jclepro.2023.137629.
[20] B. Koçak, M. Majó, C. Barreneche, A. I. Fernández, and H. Paksoy, "Performance analysis of a molten salt packed-bed thermal energy storage system using three different waste materials," *Solar Energy Materials and Solar Cells,* vol. 278, p. 113199, 2024/12/01/ 2024, doi: https://doi.org/10.1016/j.solmat.2024.113199.
[21] C. Zhang, L. Hao, H. Zheng, Y. Wu, and S. Liu, "Vanadium extraction tailings based composite phase change materials: Preparation and pore-scale simulation for packed-bed thermal energy storage systems," *Energy Conversion and Management,* vol. 370, p. 122080, 2026/12/15/ 2026, doi: https://doi.org/10.1016/j.enconman.2026.122080.
[22] B. Kocak and H. Paksoy, "Performance of laboratory scale packed-bed thermal energy storage using new demolition waste based sensible heat materials for industrial solar applications," *Solar Energy,* vol. 211, pp. 1335-1346, 2020.

[23] F. El Kouihen *et al.*, "Investigation of thermal energy storage system based on mining by-products for the recovery of Moroccan mining industrial waste heat," *Applied Thermal Engineering,* vol. 230, p. 120708, 2023.
[24] M. A. Keilany, M. Milhé, J.-J. Bézian, Q. Falcoz, and G. Flamant, "Experimental evaluation of vitrified waste as solid fillers used in thermocline thermal energy storage with parametric analysis," *Journal of Energy Storage,* vol. 29, p. 101285, 2020.
[25] P. Schwarzmayr, F. Birkelbach, H. Walter, and R. Hofmann, "Standby efficiency and thermocline degradation of a packed bed thermal energy storage: An experimental study," *Applied Energy,* vol. 337, p. 120917, 2023/05/01/ 2023, doi: https://doi.org/10.1016/j.apenergy.2023.120917.
[26] J. L. Sanz, F. C. Nuñez, and F. Zaversky, "Benchmarking analysis of a novel thermocline hybrid thermal energy storage system using steelmaking slag pebbles as packed-bed filler material for central receiver applications," *Solar Energy,* vol. 188, pp. 644-654, 2019.
[27] M. M. S. Al-Azawii, S. F. H. Alhamdi, S. Braun, J.-F. Hoffmann, N. Calvet, and R. Anderson, "Experimental study on packed-bed thermal energy storage using recycled ceramic as filler materials," *Journal of Energy Storage,* vol. 44, p. 103375, 2021/12/01/ 2021, doi: https://doi.org/10.1016/j.est.2021.103375.
[28] M. M. Al-Azawii, S. F. Alhamdi, S. Braun, J.-F. Hoffmann, N. Calvet, and R. Anderson, "Thermocline in packed bed thermal energy storage during charge-discharge cycle using recycled ceramic materials-Commercial scale designs at high temperature," *Journal of Energy Storage,* vol. 64, p. 107209, 2023.
[29] E. Papargyropoulou, C. Preece, R. Padfield, and A. A. Abdullah, "Sustainable construction waste management in Malaysia: A contractor's perspective," in *Management and Innovation for a Sustainable Built Environment MISBE 2011, Amsterdam, The Netherlands, June 20-23, 2011*, 2011: CIB, Working Commissions W55, W65, W89, W112; ENHR and AESP.
[30] B. Koçak, A. I. Fernandez, and H. Paksoy, "Long-term stability of sensible thermal energy storage materials developed from demolition wastes interacting with hot heat transfer fluid," *International Journal of Energy Research,* vol. 45, no. 15, pp. 21451-21463, 2021.
[31] M. Pires *et al.*, "Construction waste management and circular economy in urban infrastructure: a systematic literature review and strategic perspectives for emerging economies," *Journal of Building Pathology and Rehabilitation,* vol. 11, no. 3, p. 166, 2026.
[32] B. Ghorbani, A. Arulrajah, G. Narsilio, S. Horpibulsuk, and M. Leong, "Resilient moduli of demolition wastes in geothermal pavements: Experimental testing and ANFIS modelling," *Transportation Geotechnics,* vol. 29, p. 100592, 2021/07/01/ 2021, doi: https://doi.org/10.1016/j.trgeo.2021.100592.
[33] A. Arulrajah, B. Ghorbani, G. Narsilio, S. Horpibulsuk, and M. Leong, "Thermal performance of geothermal pavements constructed with demolition wastes," *Geomechanics for Energy and the Environment,* vol. 28, p. 100253, 2021/12/01/ 2021, doi: https://doi.org/10.1016/j.gete.2021.100253.
[34] P. Mikhailenko, M. Rafiq Kakar, Z. Piao, M. Bueno, and L. Poulikakos, "Incorporation of recycled concrete aggregate (RCA) fractions in semi-dense asphalt (SDA) pavements: Volumetrics, durability and mechanical properties," *Construction and Building Materials,* vol. 264, p. 120166, 2020/12/20/ 2020, doi: https://doi.org/10.1016/j.conbuildmat.2020.120166.

[35] W. Tu and M. Zhang, "Behaviour of alkali-activated concrete at elevated temperatures: A critical review," *Cement and Concrete Composites,* vol. 138, p. 104961, 2023/04/01/ 2023, doi: https://doi.org/10.1016/j.cemconcomp.2023.104961.
[36] H. K. A. Al-Bayati, P. K. Das, S. L. Tighe, and H. Baaj, "Evaluation of various treatment methods for enhancing the physical and morphological properties of coarse recycled concrete aggregate," *Construction and Building Materials,* vol. 112, pp. 284-298, 2016/06/01/ 2016, doi: https://doi.org/10.1016/j.conbuildmat.2016.02.176.
[37] I. Ramón-Álvarez, G. Moreno-Silva, E. Asensio, S. Sánchez-Delgado, and M. Torres-Carrasco, "Manufacturing and performance of eco-efficient cementitious storage tanks incorporating recycled demolition waste for thermal energy storage," *Journal of Energy Storage,* vol. 180, p. 124305, 2026.
[38] M. J. Abden, V. W. Tam, J. D. Afroze, and K. N. Le, "Innovative PCM-enhanced recycled concrete for year-round energy savings and thermal regulation in buildings," *Energy,* vol. 318, p. 134825, 2025.
[39] A. Mistri, S. K. Bhattacharyya, N. Dhami, A. Mukherjee, and S. V. Barai, "A review on different treatment methods for enhancing the properties of recycled aggregates for sustainable construction materials," *Construction and building materials,* vol. 233, p. 117894, 2020.
[40] H. Zhang, T. Ji, and H. Liu, "Performance evolution of the interfacial transition zone (ITZ) in recycled aggregate concrete under external sulfate attacks and dry-wet cycling," *Construction and Building Materials,* vol. 229, p. 116938, 2019.
[41] Y. Jiang, V. W. Y. Tam, C. Jiang, and K. N. Le, "A review on mechanical properties and durability of recycled coarse aggregate concrete exposed to elevated temperatures," *Renewable and Sustainable Energy Reviews,* vol. 217, p. 115730, 2025/07/01/ 2025, doi: https://doi.org/10.1016/j.rser.2025.115730.
[42] D. Oh, T. Noguchi, R. Kitagaki, and H. Choi, "Proposal of demolished concrete recycling system based on performance evaluation of inorganic building materials manufactured from waste concrete powder," *Renewable and Sustainable Energy Reviews,* vol. 135, p. 110147, 2021/01/01/ 2021, doi: https://doi.org/10.1016/j.rser.2020.110147.
[43] V. Arulkumar, T. Nguyen, N.-K. Bui, E. Wang, T. Ngo, and T. Noguchi, "Recovery and activation of recycled concrete powder using thermo-mechanical process," *Construction and Building Materials,* vol. 516, p. 145695, 2026/03/21/ 2026, doi: https://doi.org/10.1016/j.conbuildmat.2026.145695.
[44] L. Wu, Z. Sun, and Y. Cao, "Modification of recycled aggregate and conservation and application of recycled aggregate concrete: A review," *Construction and Building Materials,* vol. 431, p. 136567, 2024/06/14/ 2024, doi: https://doi.org/10.1016/j.conbuildmat.2024.136567.
[45] V. Arulkumar *et al.*, "Thermo-mechanical treatment for enhancing the properties of recycled concrete aggregate," *Journal of Advanced Concrete Technology,* vol. 23, no. 3, pp. 168-183, 2025.
[46] Z. Ma, R. Hu, P. Yao, and C. Wang, "Utilizing heat-mechanical synergistic treatment for separating concrete waste into high-quality recycled aggregate, active recycled powder and new concrete," *Journal of Building Engineering,* vol. 68, p. 106161, 2023/06/01/ 2023, doi: https://doi.org/10.1016/j.jobe.2023.106161.
[47] A. P. Fardnam, T. N. Nguyen, and V. Arulkumar, "Three-dimensional meso-scale finite element modeling of recycled aggregate concrete using cohesive zone method," *Structural Concrete,* 2026.

[48] K. Knobloch, T. Ulrich, C. Bahl, and K. Engelbrecht, "Degradation of a rock bed thermal energy storage system," *Applied Thermal Engineering,* vol. 214, p. 118823, 2022.
[49] E. Garitaonandia, P. Arribalzaga, I. Miguel, and D. Bielsa, "Characterization of the ratcheting effect on the filler material of a steel slag-based thermal energy storage," *Energies,* vol. 17, no. 7, p. 1515, 2024.
[50] A. Jalaeeyan and J. Zehfuß, "Experimental Investigations About the Fire Performance of Concrete with High Recycled Aggregate Content (IWCF RILEM 2025)," *Fire Technology,* vol. 62, no. 4, p. 98, 2026.
[51] L. Wei, Z. Liu, L. Li, S. Zhao, and Z. Zhang, "Thermal Degradation Mechanisms and Residual Performance of LS-GGBS-FA–Based Alkali-Activated Recycled Concrete after Exposure to Elevated Temperatures," *Journal of Materials in Civil Engineering,* vol. 38, no. 6, p. 04026146, 2026.
[52] C. Feng, W. Luo, Z. Ye, M. Du, J. Zhu, and Y. Bian, "Effect of nano silica-cement paste impregnation-carbonation reinforcement on the properties of low-quality recycled aggregates," *Construction and Building Materials,* vol. 450, p. 138619, 2024.
[53] L. Australian Steel Mill Services Pty, "What is Slag?." [Online]. Available: https://www.asms.com.au/what-is-slag.html.
[54] Y. Wang, Y. Wang, H. Li, J. Zhou, and K. Cen, "Thermal properties and friction behaviors of slag as energy storage material in concentrate solar power plants," *Solar Energy Materials and Solar Cells,* vol. 182, pp. 21-29, 2018/08/01/ 2018, doi: https://doi.org/10.1016/j.solmat.2018.03.020.
[55] I. Ramón-Álvarez, G. J. Moreno-Silva, E. Asensio, S. Sánchez-Delgado, and M. Torres-Carrasco, "Manufacturing and performance of eco-efficient cementitious storage tanks incorporating recycled demolition waste for thermal energy storage," *Journal of Energy Storage,* vol. 180, p. 124305, 2026/12/01/ 2026, doi: https://doi.org/10.1016/j.est.2026.124305.
[56] W. Bunnings, "Earthwool R4.0 Ceiling Batt 195 mm x 430 mm x 1160 mm 7.5 m² - 15 Pack URL - https://www.bunnings.com.au/earthwool-r4-0-ceiling-batt-195mm-x-430mm-x-1160mm-7-5m-15-pack_p0300790." [Online]. Available: https://www.bunnings.com.au/earthwool-r4-0-ceiling-batt-195mm-x-430mm-x-1160mm-7-5m-15-pack_p0300790.
[57] B. Xie, N. Baudin, J. Soto, Y. Fan, and L. Luo, "Experimental and numerical study on the thermocline behavior of packed-bed storage tank with sensible fillers," *Renewable Energy,* vol. 209, pp. 106-121, 2023/06/01/ 2023, doi: https://doi.org/10.1016/j.renene.2023.03.107.
[58] J.-W. Han and B.-J. Chung, "Thermal performance of a packed bed thermocline thermal energy storage system according to the design parameters," *Journal of Mechanical Science and Technology,* vol. 38, no. 8, pp. 4409-4419, 2024.
[59] X. Ma, C. Fan, W. Shao, Q. Cao, and Z. Cui, "Numerical and experimental studies of packed bed thermal energy storage system based on a novel transient energy model," *Energy Science & Engineering,* vol. 11, no. 2, pp. 727-744, 2023.
[60] H. Zhou, Z. Lai, and K. Cen, "Experimental study on energy storage performances of packed bed with different solid materials," *Energy,* vol. 246, p. 123416, 2022/05/01/ 2022, doi: https://doi.org/10.1016/j.energy.2022.123416.
[61] P. Schwarzmayr, F. Birkelbach, H. Walter, and R. Hofmann, "Exergy efficiency and thermocline degradation of a packed bed thermal energy storage in partial cycle operation: An experimental study," *Applied Energy,* vol. 360, p. 122895, 2024/04/15/ 2024, doi: https://doi.org/10.1016/j.apenergy.2024.122895.

[62] I. Ortega-Fernández *et al.*, "Operation strategies guideline for packed bed thermal energy storage systems," *International Journal of Energy Research,* vol. 43, no. 12, pp. 6211-6221, 2019.
[63] B. Xie, N. Baudin, J. Soto, Y. Fan, and L. Luo, "Wall impact on efficiency of packed-bed thermocline thermal energy storage system," *Energy,* vol. 247, p. 123503, 2022/05/15/ 2022, doi: https://doi.org/10.1016/j.energy.2022.123503.
[64] A. C. Hoffmann and H. J. Finkers, "A relation for the void fraction of randomly packed particle beds," *Powder Technology,* vol. 82, no. 2, pp. 197-203, 1995/02/01/ 1995, doi: https://doi.org/10.1016/0032-5910(94)02910-G.
[65] H. Kalman, "Effect of particle shape on void fraction," *Powder Technology,* vol. 407, p. 117665, 2022/07/01/ 2022, doi: https://doi.org/10.1016/j.powtec.2022.117665.
[66] E. B. Hassan and J. Hoffmann, "Review on pressure drop through a randomly packed bed of crushed rocks," *Discover Applied Sciences,* vol. 6, no. 3, p. 126, 2024.
[67] S. Ergun, "Fluid flow through packed columns," *Chemical engineering progress,* vol. 48, no. 2, p. 89, 1952.
[68] J. Tallmadge, "Packed bed pressure drop-an extension to higher Reynolds numbers," *AIChE J.,* vol. 16, pp. 1092-1093, 1970.
[69] D. Nemec and J. Levec, "Flow through packed bed reactors: 1. Single-phase flow," *Chemical Engineering Science,* vol. 60, no. 24, pp. 6947-6957, 2005.
[70] L. D. Harrison, K. M. Brunner, and W. C. Hecker, "A combined packed-bed friction factor equation: Extension to higher Reynolds number with wall effects," *AIChE Journal,* vol. 59, no. 3, 2013.
[71] M. Ö. Çarpinlioğlu and E. Özahi, "A simplified correlation for fixed bed pressure drop," *Powder technology,* vol. 187, no. 1, pp. 94-101, 2008.
[72] E. W. Lemmon, "NIST 72. NIST Thermophysical Properties of Air and Air Component Mixtures: AIRPROPS," 2003.
[73] X. Wang *et al.*, "Multiscale and multidimensional analysis of coarse aggregate morphological characteristics for road-used steel slag," *Construction and Building Materials,* vol. 506, p. 145025, 2026/01/13/ 2026, doi: https://doi.org/10.1016/j.conbuildmat.2025.145025.
[74] K. Ma *et al.*, "The morphological characteristics of brick-concrete recycled coarse aggregate based on the digital image processing technique," *Journal of Building Engineering,* vol. 44, p. 103292, 2021/12/01/ 2021, doi: https://doi.org/10.1016/j.jobe.2021.103292.
[75] N. Sassine, F.-V. Donzé, A. Bruch, and B. Harthong, "Numerical analysis of granular bed behavior in thermocline storage tank and bed/wall interactions," in *AIP conference proceedings*, 2018, vol. 2033, no. 1: AIP Publishing LLC, p. 090026.
[76] S.-B. Cho, J. Yoo, K. L. Frick, and S. Bragg-Sitton, "Thermomechanical analysis of packed-bed thermal-energy storage tanks: a study of design parameters affecting thermal ratcheting under thermal cycling conditions," in *19th International Topical Meeting on Nuclear Reactor Thermal Hydraulics (NURETH-19)*, 2022.
[77] J. Tang, H. Lu, X. Guo, and H. Liu, "Static wall pressure distribution characteristics in horizontal silos," *Powder Technology,* vol. 393, pp. 342-348, 2021/11/01/ 2021, doi: https://doi.org/10.1016/j.powtec.2021.07.084.
[78] S. Næss-Schmidt, H. N. Jensen, and J. Lutz, "District Heating Tariffs in Europe: Comparison of Tariffs and Regulation in Europe," Copenhagen Economics, Copenhagen, Report 2021/04/06 2021. Accessed: 2026/09/10. [Online]. Available: https://open.overheid.nl/documenten/ronl-ec66e0006b7e0acc22629091d63b448a4af5b0c3/pdf

[79] M. Hardwick and K. Joyce, "Heat Pump Project: 2021/ARP021 Final Report," Hardwick Processors Proprietary Limited, Final report 2025/06/11 2025. Accessed: 2026/09/10. [Online]. Available: https://arena.gov.au/assets/2025/08/Hardwick-Meatworks-Heat-Pump-Installation-and-Power-Upgrade-Demonstration-Final-Report.pdf

[80] G. Jia *et al.*, "Experimental and numerical investigation into a thermocline storage for district heating," *Applied Thermal Engineering,* vol. 245, p. 122748, 2024/05/15/ 2024, doi: https://doi.org/10.1016/j.applthermaleng.2024.122748.

[81] S. N. Sambo, L. Hockaday, T. Seodigeng, and Q. G. Reynolds, "Numerical and Experimental Study of Packed Bed Heat Transfer on the Preheating of Manganese Ore with Air up to 600° C," *Metals,* vol. 15, no. 3, p. 269, 2025.

[82] S. Wang *et al.*, "Thermal energy storage in concrete utilizing a thermosiphon heat exchanger," *Journal of Energy Storage,* vol. 64, p. 107201, 2023/08/01/ 2023, doi: https://doi.org/10.1016/j.est.2023.107201.

[83] I. Calderón-Vásquez *et al.*, "Review on modeling approaches for packed-bed thermal storage systems," *Renewable and Sustainable Energy Reviews,* vol. 143, p. 110902, 2021/06/01/ 2021, doi: https://doi.org/10.1016/j.rser.2021.110902.

[84] T. The Engineering, "Fans - Efficiency and Power Consumption," 2003. [Online]. Available: https://www.engineeringtoolbox.com/fans-efficiency-power-consumption-d_197.html.

[85] A. Mistri, T. Roy, and B. Bhattacharjee, "A review on recycled concrete aggregate (RCA) properties and enhancement techniques," *Construction and Building Materials,* 2022. [Online]. Available: https://doi.org/10.1016/j.conbuildmat.2022.126699.

[86] M. N. Strasser and R. P. Selvam, "A cost and performance comparison of packed bed and structured thermocline thermal energy storage systems," *Solar Energy,* vol. 108, pp. 390-402, 2014/10/01/ 2014, doi: https://doi.org/10.1016/j.solener.2014.07.023.

[87] M. M. S. Al-Azawii, S. F. H. Alhamdi, S. Braun, J.-F. Hoffmann, N. Calvet, and R. Anderson, "Thermocline in packed bed thermal energy storage during charge-discharge cycle using recycled ceramic materials - Commercial scale designs at high temperature," *Journal of Energy Storage,* vol. 64, p. 107209, 2023/08/01/ 2023, doi: https://doi.org/10.1016/j.est.2023.107209.

[88] Z. Zeng, B. Zhao, and R. Wang, "High-power-density packed-bed thermal energy storage using form-stable expanded graphite-based phase change composite," *Renewable and Sustainable Energy Reviews,* vol. 182, p. 113373, 2023/08/01/ 2023, doi: https://doi.org/10.1016/j.rser.2023.113373.

[89] M. Aggregate. "Slag 2 to 4 inch (4x2 Slag) – Product Information and Pricing." Aggregate Markets. https://aggregatemarkets.com/en/products/slag/4x2-slag (accessed.

[90] Echemi. "Stearic Acid Price and Market Analysis." https://www.echemi.com/productsInformation/pid_Seven41144-stearicacid.html (accessed.

[91] F. Gong, Z. Wang, L. Yang, Q. Wu, Y. Ning, and Q. Zeng, "Effect of original mix proportion on rapid removing of attached mortar for recycled concrete aggregate through a freeze-thaw approach," *Journal of Advanced Concrete Technology,* vol. 21, no. 6, pp. 477-491, 2023.

[92] Q. Wu, F. Gong, D. Zhi, and Y. Zhao, "Removing attached mortar from recycled aggregate by the combined freeze–thaw cycles and high-temperature drying," *Structural Concrete,* vol. 23, no. 5, pp. 3126-3139, 2022.